Cationic Polymer-Coated Magnetic Nanoparticles for the Separation and Detection of Bacterial Contamination in food samples

KAMONLUCK WITTHAYASUTTHAPHON

A THESIS SUBMITTED IN PARTIAL FULFILLMENT OF
THE REQUIREMENTS FOR MASTER DEGREE OF SCIENCE
IN CHEMISTRY
FACULTY OF SCIENCE
BURAPHA UNIVERSITY
2024

อนุภาคนาโนแม่เหล็กเคลือบด้วยพอลิเมอร์ประจุบวกสำหรับการแยกและตรวจวัดการปนเปื้อนแบคทีเรียในตัวอย่างอาหาร

กมลลักษณ์ วิทยสุทธาพร

วิทยานิพนธ์นี้เป็นส่วนหนึ่งของการศึกษาตามหลักสูตรวิทยาศาสตรมหาบัณฑิต
สาขาวิชาเคมี
คณะวิทยาศาสตร์ มหาวิทยาลัยบูรพา
2567

Cationic Polymer-Coated Magnetic Nanoparticles for the Separation and Detection of Bacterial Contamination in food samples

KAMONLUCK WITTHAYASUTTHAPHON

A THESIS SUBMITTED IN PARTIAL FULFILLMENT OF
THE REQUIREMENTS FOR MASTER DEGREE OF SCIENCE
IN CHEMISTRY
FACULTY OF SCIENCE
BURAPHA UNIVERSITY
2024

The Thesis of Kamonluck Witthayasutthaphon has been approved by the examining committee to be partial fulfillment of the requirements for the Master Degree of Science in Chemistry of Burapha University

Advisory Committee

Principal advisor

.....

(Associate Professor Dr. Thanida Trakulsujaritchok)

Co-advisor

.....

(Dr. Yothin Teethaisong)

Examining Committee

..... Principal examiner

(Assistant Professor Dr. Anyarat Watthanaphanit)

..... Member

(Assistant Professor Dr. Piyaporn Nanongkhai)

..... Member

(Dr. Yothin Teethaisong)

..... Member

(Associate Professor Dr. Thanida Trakulsujaritchok)

..... Dean of the Faculty of Science

(Associate Professor Dr. Usavadee Tuntiwaranuruk)

.....

This Thesis has been approved by Graduate School Burapha University to be partial fulfillment of the requirements for the Master Degree of Science in Chemistry of Burapha University

..... Dean of Graduate School

(Associate Professor Dr. Witawat Jangiam)

.....

65910110: MAJOR: CHEMISTRY; M.Sc. (CHEMISTRY)

KEYWORDS: MAGNETIC NANOPARTICLES; CHITOSAN; TOTAL BACTERIA COUNT (TBC); PORTABLE GLUCOSE METER (PGMS)

KAMONLUCK WITTHAYASUTTHAPHON : CATIONIC POLYMER-COATED MAGNETIC NANOPARTICLES FOR THE SEPARATION AND DETECTION OF BACTERIAL CONTAMINATION IN FOOD SAMPLES. ADVISORY COMMITTEE: THANIDA TRAKULSUJARITCHOK, Ph.D. YOTHIN TEETHAISONG, Ph.D. 2024.

Rapid and high-efficiency measurement of bacteria can help prevent foodborne diseases. In this research, a simple method was devised for detecting the total bacteria count in food samples, employing an integrated approach with chitosan-coated magnetic nanoparticles for bacteria capture and a portable glucose meter (PGM) for detection readout. Magnetic nanoparticles (MNPs) were first synthesized using the co-precipitation of Fe^{2+} and Fe^{3+} in the presence of NH_4OH. To increase nanoparticles stability, citric acid was added after MNPs formation. The MNPs are subsequently coated with chitosan polymer using two approaches: 1) electrostatic adsorption, resulting in MNPs-CH, and 2) chemical bonding, resulting in MNPs-PDA-CH. Both MNPs-CH and MNPs-PDA-CH were characterized using various techniques such as ATR-FTIR, TEM, Zeta-potential, and EDX. After being coated with chitosan, the surface charge of MNPs changed from negative to positive, making them suitable for bacteria capture. Both MNPs-CH and MNPs-PDA-CH demonstrated strong capture capabilities for *Escherichia coli* and *Staphylococcus aureus* through electrostatic adsorption between the positively charged nanoparticles and the negatively charged bacteria. Subsequently, the captured bacteria could be detected using PGMs. The decrease in glucose consumption by bacteria was proportional to the concentration of bacteria, with a good linear range. This method demonstrates good detection performance for both gram-negative *Escherichia coli* and gram-positive *Staphylococcus aureus* in dried seafood samples. The detection accuracy in real samples is 95%. By measuring the glucose consumption by bacteria, this method offers a simple and cost-effective means of detecting the total bacteria count in food and environmental samples.

มหาวิทยาลัยบูรพา
BURAPHA UNIVERSITY

ACKNOWLEDGEMENTS

First of all, I extend my heartfelt gratitude and sincere appreciation to my advisor and co-Advisor, Assoc. Prof. Dr. Thanida Trakulsujaritchok and Dr. Yothin Teethaisong for their invaluable guidance, unwavering support, encouragement, and insightful advice throughout my study and research journey. Great appreciation is offered to all committee members for thesis defense, Asst. Prof. Dr. Piyaporn Na Nongkhai and Asst. Prof. Dr. Anyarat Watthanaphanit for valuable feedback, suggestions, and insights, as well as addressing any shortcomings, significantly enhances the completeness of this thesis.

I would like to acknowledge (i) Scholarship Support from Burapha University (ii) the Center of Excellence for Innovation in Chemistry (PERCH-CIC), Commission on Higher Education, Ministry of Education, Thailand (iii) Science Innovation Facility, Faculty of Science, Burapha University for the supports throughout my research. I also would like to thank the Department of Chemistry, Faculty of Science, Burapha University, Thailand where I obtained very good experiences.

I express my sinclair to the lecturers in the Chemistry Department, Faculty of Science who helps teach and teach the content of the chemistry subject and conduct chemical operations with intensity and care in order to grow me into a good and qualified scientist.

Finally, I would like to express my gratitude to my father, mother, family and

Miss. Varunee Sadsri for their unwavering support and encouragement in every aspect of my life. The value and benefits of this thesis I would like to express my gratitude to my parents, ancestors, and all benefactors both past and present. Their support has played a crucial role in shaping me into the educated and successful person I am today.

Kamonluck Witthayasutthaphon

TABLE OF CONTENTS

Page

ABSTRACT ..... D

ACKNOWLEDGEMENTS ..... F

TABLE OF CONTENTS ..... G

LIST OF TABLE ..... J

LIST OF FIGURE ..... K

CHAPTER 1 1

INTRODUTION 1

1.1 Background 1

1.2 Objectives 3

1.3 Contribution to knowledge 3

1.4 Scope to study 3

CHAPTER 2 4

LITERATURE REVIEW 4

2.1 Iron (III) oxide nanoparticles 4

2.2 Polydopamine 7

2.3 Cationic polymer 9

2.4 Literature review of polydopamine modified iron (III) oxide nanoparticles 10

2.5 Literature review of iron (III) oxide nanoparticles for bacteria separation 11

2.6 Detection of bacteria using PGM-based method. 14

CHAPTER 3 18

EXPERIMENTALS 18

3.1 Materials 18

3.2 Bacteria and culture conditions 19

3.3 Instrument 19

3.4 Experimental section 20

3.4.1 Synthesis of magnetite nanoparticle (MNPs) 20
3.4.2 For electrostatic adsorption 21
3.4.2.1 Preparation of Chitosan modified MNPs (MNPs-CH) 21
3.4.3 For covalent adsorption 22
3.4.3.1 Synthesis of polydopamine coated MNPs (MNPs-PDA) 22
3.4.3.2 Preparation of Chitosan modified MNPs-PDA (MNPs-PDA-CH) 23
3.4.4 Examination of bacterial separation 24
3.4.4.1 Bacterial culture 24
3.4.4.2 Separation of bacteria with MNPs-PDA-CH and MNPs-CH 24
3.4.5 Detection of bacteria using magnetic nanoparticles in combination with a glucometer 24
3.4.5.1 Preparation of Escherichia coli ATCC 25922 24
3.4.5.2 Preparation of Staphylococcus aureus ATCC 29213 25
3.4.5.3 Detection procedure 25
3.4.6 Detection of bacteria in dried seafood 26
CHAPTER 4 27
RESULTS AND DISCUSSION 27
4.1 Synthesis of magnetic nanoparticle (MNPs) 27
4.2 Preparation of Chitosan modified MNPs (MNPs-CH) via electrostatic adsorption method 29
4.3 Preparation of Chitosan modified MNPs (MNPs-PDA-CH) via covalent adsorption method 34
4.3.1 Synthesis of polydopamine coated MNPs (MNPs-PDA) 34
4.3.2 Preparation of Chitosan modified MNPs-PDA (MNPs-PDA-CH) 39
4.4. Isoelectric Point Determination of MNPs-CH and MNPs-PDA-CH 42
4.5 The study of bacteria separation 43
4.6 The study of bacteria detection 45
4.6.1 Optimization of experiment parameters 47
4.6.1.1 Effect of nanoparticles type 47

4.6.1.2 Effect of nanoparticles amount....49
4.6.1.3 Effect of the sample volume....50
4.6.1.4 Effect of incubation time of MNPs-PDA-CH with bacteria....51
4.7 The study of bacteria detection in real sample....52
4.7.1 Detection of E. coli in dried shrimp....52
4.7.1 Detection of S. aureus in dried shrimp....54
4.8 Method validation....55
CHAPTER 5....61
CONCLUSION AND DISCUSSION....61
REFERENCES....62
BIOGRAPHY....65

LIST OF TABLE

Page

Table 2-1 The main fields where IONPs have been employed (Ali et al., 2016). 5

Table 4-1 Performance evaluation of total bacteria count in real samples. 56

Table 4-2 Results of testing efficiency for measuring total bacteria in dried ink samples. Comparison between the standard method (plate culture) and the new method for measuring bacteria (our method).....57

Table 4-3 Results of testing efficiency for measuring total bacteria in dried shrimp samples. Comparison between the standard method (plate culture) and the new method for measuring bacteria (our method).....59

LIST OF FIGURE

Page

Figure 1-1 The proposed portable glucose meters (PGMs) for bacteria detection. 3

Figure 2-1 Possible crystal structures of the Iron Oxides Nanoparticles (IONPs). 6

Figure 2-2 Magnetization curves of (a) MNPs and (b) MNPs@PDA 7

Figure 2-3 (a) The initial stages of the formation of polydopamine and (b) Molecular structures of polydopamine. 8

Figure 2-4 The immobilization of biomolecules with thiol (a) and amino (b) groups by Michael addition and Schiff base reaction. 9

Figure 2-5 Illustration of chitosan versatility. 10

Figure 2-6 The synthesis of magnetic nanoparticles covered with PDA and loaded with doxorubicin (red molecule) (Mrówczyński et al., 2016). 10

Figure 2-7 Reaction steps for the preparation of β-CD-functionalized magnetic nanoparticles (β-CD-PDA-MNPs) 11

Figure 2-8 The magnetic nanoparticle-based separation of bacteria from a contaminated solution (Augustine, Abraham, Kalarikkal, & Thomas, 2016) 12

Figure 2-9 Schematic representation of Fe_3O_4@sSiO_2-PEI (PEI-MNPs) nanoparticles modification and Fe_3O_4@sSiO_2-NH_2 (NH-MNPs) nanoparticles catch pathogenic bacteria (Fang et al., 2016). 13

Figure 2-10 Illustration depicts the steps involved in the capture of bacteria with NP^+ and NP^- (Z. Li et al., 2019). 13

Figure 2-11 Schematic representation of enrichment and detection of bacteria using Fe_3O_4@PDA@PEI MBs (Zhang et al., 2022). 14

Figure 2-12 Schematic of the detection of *Salmonella* bacteria experimental procedure using a PGM (Joo et al., 2013). 15

Figure 2-13 Schematic representation of the detection process: (a) Initial readings of the mixture taken immediately after the addition of glucose (T = 0 h) (b) readings taken after 'T' hours depending on the level of contamination of the water samples (Chavali, Kumar Gunda, Naicker, & Mitra, 2014). 16

Figure 2-14 Schematic of the detection procedure for *C. sakazakii* using SiNP-GOX-IgG, MNP-IgG typical sandwich feature and PGM (Ye, Zhao, & Dou, 2017) 17

Figure 2-15 The process of enrofloxacin detection in a test sample solution containing glucose and *E. coli*, using either a personal glucose meter or glucose paper test strips (Kwon et al., 2018). 17

Figure 3-1 Illustrates the steps in measuring bacteria using a glucose meter. 26

Figure 4-1 ATR-FTIR spectra of citric-stabilized MNPs..... 28

Figure 4-2 TEM image of MNPs-Citric..... 28

Figure 4-3 Magnetic properties image of MNPs-Citric..... 28

Figure 4-4 EDX analysis of MNPs-Citric..... 29

Figure 4-5 Illustrates the preparation of chitosan-modified MNPs (MNPs-CH) 29

Figure 4-6 ATR-FTIR spectra of MNPs-Citric modified with chitosan 30

Figure 4-7 TEM image of (a) MNPs-Citric, (b) MNPs-CH 62.5 mg , (c) MNPs-CH 125 mg and (d) MNPs-CH 250 mg..... 31

Figure 4-8 Hydrodynamic diameter of MNPs-Citric and MNPs-CH with various concentrations of chitosan. The data were expressed as mean ± SD. 32

Figure 4-9 Zeta potential analysis of MNPs-Citric and MNPs-CH with various 32

Figure 4-10 Magnetic properties image of (a) MNPs-CH 62.5 mg, (b) MNPs-CH 125 mg and (c) MNPs-CH 250 mg..... 33

Figure 4-11 Illustrates the preparation of polydopamine-modified MNPs (MNPs-PDA) 34

Figure 4-12 ATR-FTIR spectra of MNPs-citric and MNPs-PDA..... 35

Figure 4-13 ATR-FTIR spectra of polymerization time 1 to 24 hours of dopamine monomer. 36

Figure 4-14 Zeta potential of MNPs-PDA with difference polymerization time 37

Figure 4-15 TEM image of MNPs-PDA 16 hours 37

Figure 4-16 Hydrodynamic diameter of MNPs-PDA with difference polymerization time. The data were expressed as mean ± SD 38

Figure 4-17 Illustrates the preparation of chitosan-modified MNPs-PDA (MNPs-PDA-CH) 39

Figure 4-18 ATR-FTIR spectra of MNPs-PDA-CH 40

Figure 4-19 Zeta potential analysis of optimum concentration with chitosan..... 40

Figure 4-20 TEM image of (a) MNPs-PDA-CH 62.5 mg, (b) MNPs-PDA-CH 125 mg and (c) MNPs-PDA-CH 250 mg..... 41

Figure 4-21 Hydrodynamic diameter of optimum concentration. 42

Figure 4-22 Isoelectric point of MNPs-CH and MNPs-PDA-CH 43

Figure 4-23 Effect of pH buffer of PBS (a) *E.coli* and (b) *S. aureus*.....44

Figure 4-24 Effect of chitosan concentration on the separation efficiency (a) MNPs-CH and (b) MNPs-PDA-CH. 45

Figure 4-25 The capture of bacteria with MNPs and the monitoring of glucose consumption by captured bacteria using a portable glucose meter (PGMs) as a signal readout. 46

Figure 4-26 The change in glucose levels in the reaction solution monitored over time by PMG. (a) *E. coli* and (b) *S. aureus*. 47

Figure 4-27 (a) Drop in PMG readings consumption by *E. coli* recorded over time for different types of nanoparticles. (b) Comparison of the %ΔC for different types of particles at 30-minute of detection time. 48

Figure 4-28 (a) Drop in PMG readings consumption by *S. aureus* recorded over time for different types of particles. (b) Comparison of the %ΔC for different types of particles at 30-minute of detection time. 48

Figure 4-29 (a) Drop in PMG readings consumption by *E. coli* recorded over time for different MNPs dosages. (b) Comparison of the %ΔC for different MNPs dosages at 8 hours of detection time. 49

Figure 4-30 (a) Drop in PMG readings consumption by *S. aureus* recorded over time different MNPs dosages. (b) Comparison of the %ΔC for different MNPs dosages at 8 hours of detection time. 49

Figure 4-31 (a) Drop in PMG readings consumption by *E. coli* recorded over time for different sample volume. (b) Comparison of the %ΔC for different sample volume at 30-minute of detection time. 50

Figure 4-32 (a) Drop in PMG readings consumption by *S. aureus* recorded over time for different sample volume. (b) Comparison of the %ΔC for different sample volume at 30-minute of detection time. 50

Figure 4-33 (a) Declining in PMG readings consumption by *E. coli* recorded over time for different incubation time of MNPs-PDA-CH with bacteria. (b) Comparison of the %ΔC for different incubation time of MNPs-PDA-CH with bacteria at 6 hours of detection time.....51

Figure 4-34 (a) Declining in PMG readings consumption by *S. aureus* recorded over time for different incubation time of MNPs-PDA-CH with bacteria. (b)

Comparison of the %ΔC for different incubation time of MNPs-PDA-CH with bacteria at 6 hours of detection time. 51

Figure 4-35 The change in glucose levels in the reaction solution monitored over time by PMG. The concentration of *E. coli* ranging from 3.25×10^1 - 3.25×10^8 CFU/mL. 53

Figure 4-36 Time needed to detect a significant decrease in glucose concentrations at various concentrations of *E. coli* ranging from 3.25×10^1 – 3.25×10^8 CFU/mL. 53

Figure 4-37 The change in glucose levels in the reaction solution monitored over time by PMG. The concentration of *S. aureus* ranging from 2.85×10^1 - 2.85×10^8 CFU/mL. 54

Figure 4-38 Time needed to detect a significant decrease in glucose concentrations at various concentrations of *S. aureus* ranging from 2.85×10^1 - 2.85×10^8 CFU/mL. 55

CHAPTER 1
INTRODUTION

1.1 Background

The presence of bacterial contaminants in food poses a significant threat to human health as it can lead to the development of numerous diseases. It is considered as one of the most significant existing problems worldwide which those often encountered include: gram-negative and gram-positive bacteria (Agyarkwa et al., 2022). Various techniques can be used for detection of bacteria, including the plate colony counting method (Clausen et al., 2018; Z. Li, Ma, Ruan, & Zhuang, 2019), as well as the multiplex polymerase chain reaction (PCR) assay (Q. Li, Xie, Wang, Aguilar, & Xu, 2021; Moffa et al., 2020), immunology-based methods (Kumar et al., 2020) etc. The drawbacks of these methods include prolonged detection time, restricted access to specialized laboratory inspection facilities, and an inability to provide real-time and on-site bacterial detection. Therefore, a simple, rapid, sensitive, and reliable screening method is still required for effective disease prevention and treatment.

Recently, magnetic nanoparticles (MNPs), particularly magnetite nanoparticles (Fe_3O_4NPs) have been subjected of extensive research due to their superparamagnetic properties, biocompatibility, and low toxicity. MNPs are especially utilized in biosensor applications to separate and capture target biomolecules, such as biomarker proteins and bacteria. Subsequently, the signal can be detected using additional amplification methods such as colorimetry, fluorescence, immunosorbent assay (ELISA), positron emission tomography (PET) (Xu et al., 2018) and magnetic resonance imaging (MRI). The separation of bacteria with MNPs has been widely used in the enrichment of targeted bacteria in which the low concentrations of bacteria in the environment could be detected (Che, Xu, Wang, & Chen, 2017; Fang et al., 2016; Z. Li et al., 2019; Meng, Li, Li, Xiong, & Xu, 2017). Electrostatic adsorption is the predominant method for separating bacteria using MNPs. Through this process, negatively charged bacteria adhere to positively charged nanocomposites via electrostatic interaction. Several studies have shown that MNPs modified with

cationic polymers can effectively separate a variety of bacteria. Increasing electrostatic interaction has been found to enhance bacteria enrichment (Clausen et al., 2018; Xiao, Bai, Wang, Sun, & Xu, 2022; Zhang et al., 2022). For example, it was demonstrated that the positive charge of self-made core-shell Fe_3O_4@Polydopamine@Polyethyleneimine magnetic beads (Fe_3O_4@PDA@PEI MBs) can be utilized as adsorbents for the broad-spectrum separation of bacteria via the electrostatic interaction. The bacteria were then easily separated from the solution by applying an external magnetic field and subsequently detected using PCR and capillary electrophoresis (CE) techniques.

Inspired by previous studies, our proposal aims to utilize chitosan, a polycationic biopolymer, to modify the surface of MNPs for capturing bacteria. Furthermore, we also aim to develop a novel approach for detecting bacteria by employing cationic-coated MNPs to separate and concentrate bacterial contamination in food samples, followed by detection using portable glucose meters (PGMs). Our focus lies in investigating the modification and application of MNPs for bacteria detection. Initially, MNPs are synthesized using the chemical co-precipitation method and subsequently modified with the positively charged polymer chitosan through two approaches: (1) electrostatic adsorption and (2) covalent bonding. We examined the effectiveness of separating both gram-negative and gram-positive bacteria using cationic-coated MNPs. Bacterial detection was assessed based on glucose consumption by captured bacteria using portable glucose meters (PGMs) as signal readers. This method enables simple, quantitative, and cost-effective detection of the total bacterial count in food samples. It is highly portable and facilitates on-site screening tests.

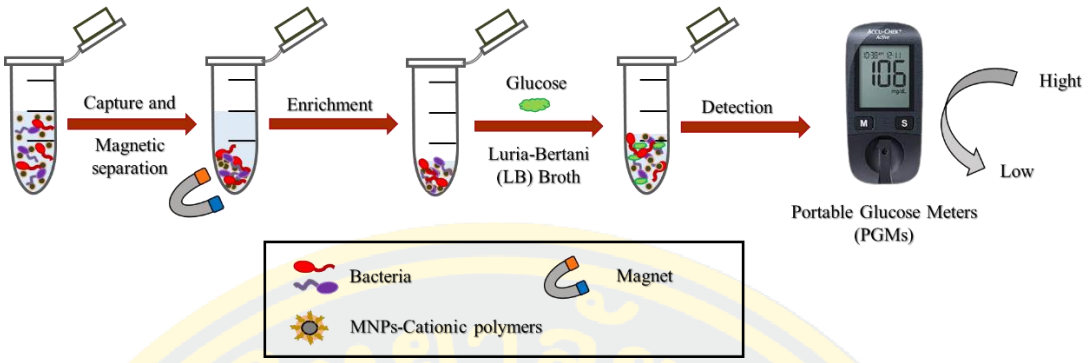

Figure 1-1 The proposed portable glucose meters (PGMs) for bacteria detection.

1.2 Objectives

To study the synthesis and modification of MNPs with chitosan

To study the detection of bacterial contamination in food samples, utilized a combination of chitosan-modified MNPs and portable glucose meters (PGMs)

1.3 Contribution to knowledge

The newly developed assay has the ability to detect various bacterial species in food, water, and other samples, and its use permits quantitative diagnostics.

1.4 Scope to study

1. Synthesis of MNPs via co-precipitation method.
2. Modification of MNPs with chitosan.
3. Characterization of chitosan modified-MNPs with various techniques.
4. Investigation of bacteria separation with chitosan modified-MNPs.
5. Examination of bacteria detection based on portable glucose meters (PGMs).

CHAPTER 2
LITERATURE REVIEW

2.1 Iron (III) oxide nanoparticles

Iron (III) oxide nanoparticles (IONPs) have gained significant attention in nanotechnology due to their superparamagnetic properties and biocompatibility. These inorganic nanomaterials are widely used and economical. IONPs find applications in various fields such as catalysts, thermite, pigments, and hemoglobin. Table 2-1 shows the summarization of the possible applications of IONPs (Ali et al., 2016). Magnetite (Fe_3O_4), maghemite (γ-Fe_2O_3), and hematite (α-Fe_2O_3) are three forms in nature of IONPs. The presence of iron cations in two valence states, Fe^{2+} and Fe^{3+}, in the inverse spinel structure of magnetite (Figure 2-1) gives it the most fascinating properties (Kuchma, Kubrin, & Soldatov, 2018).

Table 1-1 The main fields where IONPs have been employed (Ali et al., 2016).

Fields	Applications of magnetic NPs
Biomedical	Magnetic NPs (particularly coated with liposomes) for drug delivery, magnetic hyperthermia, MRI contrast agent, magnetic separation, controlled drug release, cellular therapy, eg, cell labeling, tissue repair, cell separation and handling of cells, purifying cell populations, magnetofection, diseases of the musculoskeletal system, severe inflammation, disability, and pain
Health care	Therapeutic targets in chemotherapy (cancer and tumor); nanoscale biosensors and imaging; nanocoatings on surfaces; implants; nanocarrier for vaccination; antimicrobial activities; SLN in drug delivery and research; nanophotothermolysis with pulsed lasers for the treatment of cancer, hepatitis B virus, respiratory syncytial virus, influenza virus, antiviral agents against HIV-1, monkeypox virus, herpes simplex virus type 1, and Tacaribe virus; delivering antigens for a particular disease into the blood stream; preventing aging of the skin
Agriculture and food	Nano-based products (nanofertilizers, nanofungicides, nanopesticides), engineered NPs, and CNTs boost crop yields; pyrite NPs are used as a seed treatment for various plants prior to sowing the seeds. Broader leaf morphology, larger leaf numbers, increased biomass. Enhanced breakdown of stored starch. This raises the possibility of developing iron pyrite NPs as a commercial seed treatment agent (pro-fertilizer). The strategy is safe, as the process does not put NPs into the soil. Reduced dose requirement as compared to chemical fertilizers. No adverse effects on plant growth. Nanosensors, nanofood, encapsulation, food packing, nanocoatings, precision farming (remote-sensing devices), nanocomposites, gene transfer (crop improvement), and nanoporous membranes
Environmental remediation	Pollution prevention (detection, monitoring, and remediation). Waste water treatment (permeable reactive barriers, membrane filtration, adsorption). Catalyst coatings such as palladium (Pd), climate change (carbon capture), artificial leaf for CO_2 sequestration, mineral carbonation, biomimetic carbonation, N_2O decomposition, methane combustion. Improves manufacturing processes (efficiency, waste reduction), dematerialization (reduction in material quantity), sensing (pollutant sensors, nanoporous membranes, chemical and bio-nanosensors, nanowire sensor for explosives), and energy (heat distribution, eg, ceramic-like materials that provide sufficient reliability and durability of the entire structure)
Energy	Photovoltaic film coatings, improved efficiency of fuel production and consumption, fuel cells and batteries, nanobioengineering of enzymes, thermoelectric materials, and prototype solar panels, batteries, aerogels, conversion of waste heat in computers, automobiles, homes, power plants, etc, to usable electrical power
Defense and aerospace	Nanocomposites, nanocoatings, sensors and electronics, fuel additives and energy devices, and smart materials
Construction	Nanocoatings, nanocomposites, nanoscale sensors, smart materials, and additives to concrete. Iron oxide pigments are used in coloring concrete, brick, tile, and other construction materials
Automotive	Additives in catalysts and lubricants, nanocoatings, fuel cells, composite fillers, and smart materials
Textiles	Sensors, nanofibers, coatings, and smart materials
Electronics	Printed electronics, carbon nanotubes, nanoscale memory, nanowires, NEMS, spintronics, and quantum dots

Abbreviations: CNTs, carbon nanotubes; MRI, magnetic resonance imaging; NEMS, nanoelectromechanical systems; NPs, nanoparticles; SLN, solid lipid NPs.

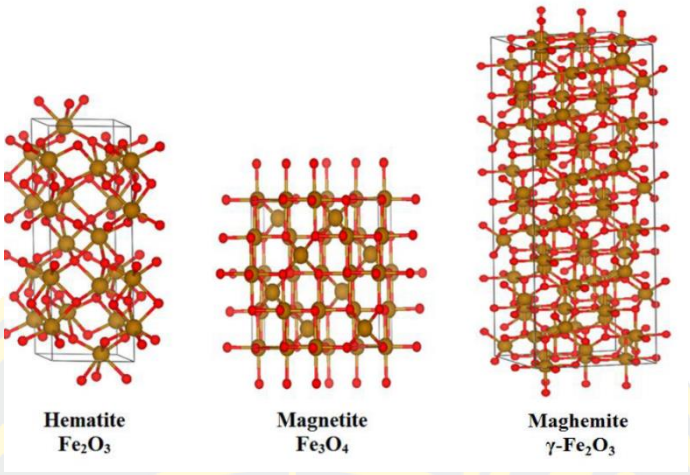

Figure 2-1 Possible crystal structures of the Iron Oxides Nanoparticles (IONPs).

IONPs with suitable surface chemistry can be prepared using various methods, such as sol-gel, hydrothermal, ultrasound irradiation, and chemical coprecipitation (Ali et al., 2016). Chemical synthesis methods are often preferred because they offer low cost and high yield. The most straightforward method of synthesizing MNPs with sizes ranging from 3 to 20 nm in diameter is chemical coprecipitation. In this method, magnetite is synthesized by adding a base solution such as ammonium hydroxide (NH_4OH) to an aqueous mixture of ferric (Fe^{2+}) and ferrous (Fe^{3+}) ions chloride at a 1:2 molar ratio, resulting in a black color. Equation 1 represents the chemical reaction of MNPs precipitation.

$$Fe^{2+} + 2Fe^{3+} + 8OH \longrightarrow Fe_3O_4 + 4H_2O \qquad (1)$$

MNPs can be completely precipitated under an oxygen-free environment at a pH between 9 and 14, with a Fe^{3+}: Fe^{2+} molar ratio of 2:1. Otherwise, might also be oxidized of MNPs as

$$Fe_3O_4 + 0.25O_2 + 4.5H_2O \longrightarrow 3Fe(OH)^{3+} \qquad (2)$$

MNPs are typically coated with stabilizer molecules to prevent oxidation and agglomeration. It is necessary to synthesize them in an oxygen-free environment,

preferably with N_2 or Ar_2 gas present. The gas not only prevents oxidation of MNPs, but also helps to reduce their size.

Magnetization curves of MNPs show in Figure 2-2 (Davodi, Jahangiri, & Ghorbani, 2018). Symmetric hysteresis and saturation magnetization can be observed exhibiting typical superparamagnetic behavior. The digital images captured the behavior of MNPs in an aquatic dispersion and during magnetic isolation. When exposed to an external magnetic field, the particles were quickly separated and could be easily re-dispersed with a gentle shake once the field was removed. This characteristic simplifies the collection, regeneration, and reuse of the particles.

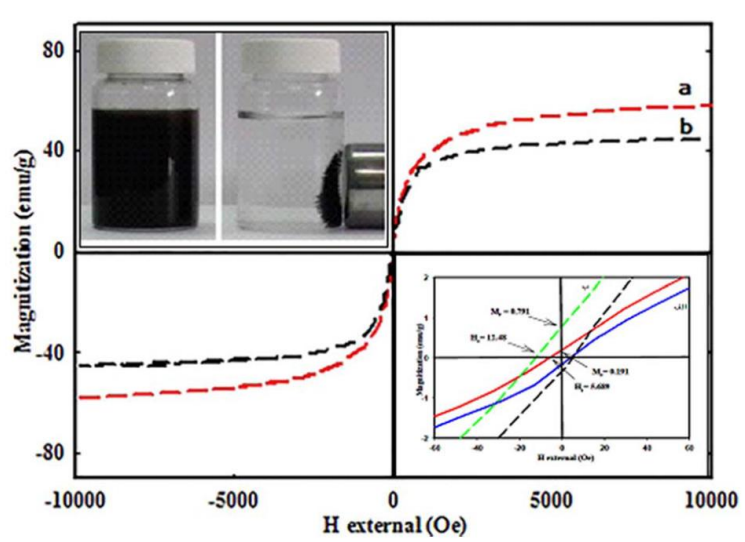

Figure 2-2 Magnetization curves of (a) MNPs and (b) MNPs@PDA (Davodi et al., 2018)

2.2 Polydopamine

Polydopamine (PDA), a synthetic version of the adhesive foot protein found in marine mussels, can efficiently modify a wide range of surfaces, both organic and inorganic, including noble metals, metals with native oxide surfaces, semiconductors, ceramics, and more. The self-polymerization of dopamine (DA) induced by oxidants, as illustrated in Figure 2-3, offers several advantages for surface functionalization, including the use of simple ingredients, mild reaction conditions, and a one-step process at room temperature (Salazar, 2016). Using PDA as an immobilization matrix offers an additional significant advantage: the covalent bonding created is relatively

stable. This contrasts with commonly used immobilization agents like N-hydroxysuccinimide (NHS) or maleimide agents, which can be less stable.

Moreover, the PDA layer has the potential to function as a versatile platform for secondary reactions. The metal-binding properties of both the catechol and nitrogen-containing groups present in the PDA structure can be utilized to achieve uniform, continuous, compact, and adhesive deposition of metal coatings on various substrates through electroless plating techniques, as demonstrated in Figure 2-4 (Davodi et al., 2018).

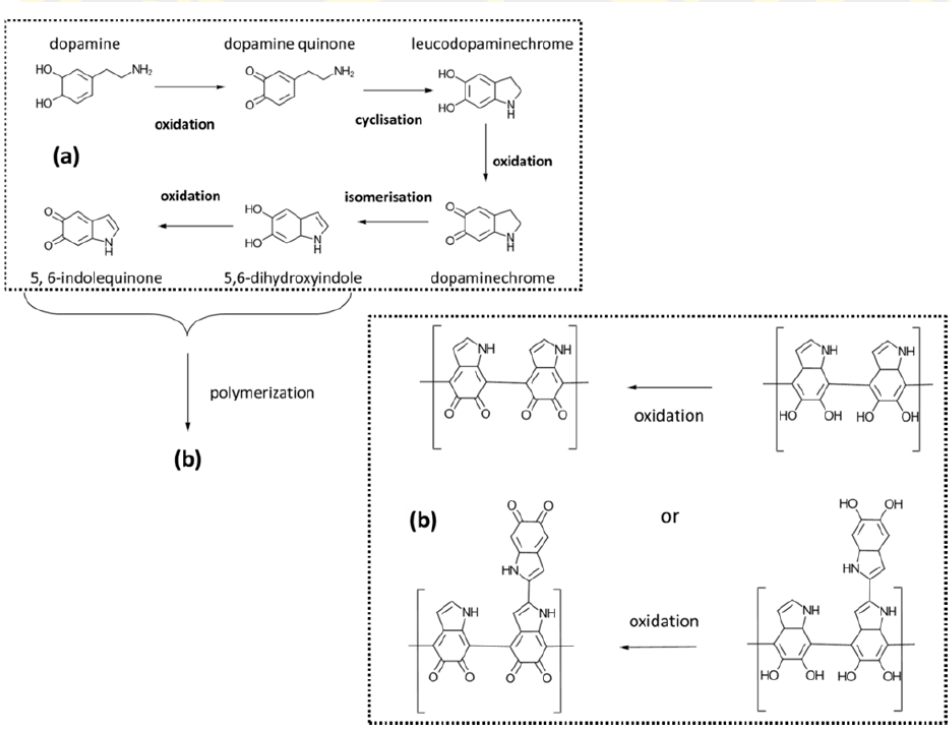

Figure 2-3 (a) The initial stages of the formation of polydopamine and (b) Molecular structures of polydopamine.

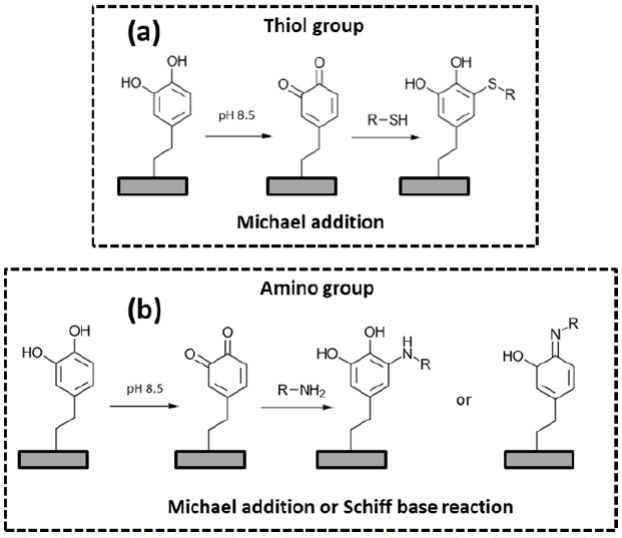

Figure 2-4 The immobilization of biomolecules with thiol (a) and amino (b) groups by Michael addition and Schiff base reaction.

2.3 Cationic polymer

Cationic polymers are widely used in various fields for their ability to carry a positive charge, which allows them to interact with negatively charged molecules such as DNA, RNA, and proteins. They are commonly used in gene therapy and drug delivery systems as they can condense nucleic acids and protect them from degradation in the bloodstream. They are also used in water treatment processes to remove impurities in the paper industry to improve the strength and stability of paper products. Additionally, cationic polymers have applications studied and utilized for bacterial capture due to their positive charge, which can attract and bind to the negatively charged bacterial cell surface. These polymers can form complexes with bacteria, leading to their precipitation or aggregation, making it easier to separate the bacterial cells from a sample. Additionally, cationic polymers can be functionalized with other groups, such as chitosan or peptides, to enhance their antibacterial activity or selectivity towards specific bacterial strains. Overall, cationic polymers show promise as a tool for bacterial capture and purification in various applications, such as water treatment and medical diagnostics.

Chitosan, a polysaccharide, has received special attention due to its natural amino polymer composition, which consists of N-acetyl glucosamine and D-glucosamine randomly distributed. This polymer has various properties, such as

biocompatibility, non-toxicity, degradability, antibacterial activity, antioxidant effect, and adhesion properties, which make it suitable for various applications. The solubility of chitosan is pH-dependent, with a response similar to that of weak acids, as depicted in Figure 2-5.

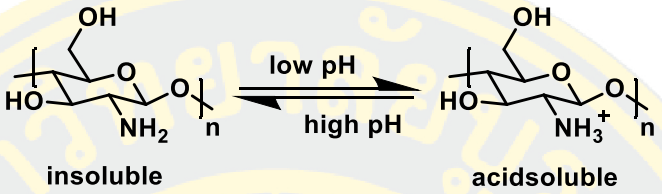

Figure 2-5 Illustration of chitosan versatility.

2.4 Literature review of polydopamine modified iron (III) oxide nanoparticles

In 2016, Mr´owczy´nski, R., et al. showed that MNP1 was synthesized using the co-precipitation method. Then, polydopamine was coated onto the surface of the nanoparticles by oxidative polymerization of dopamine under basic conditions as shown in Figure 2-6. Furthermore, it is possible to load the anticancer drug doxorubicin onto MNP1 using Michael addition and Schiff base reaction.

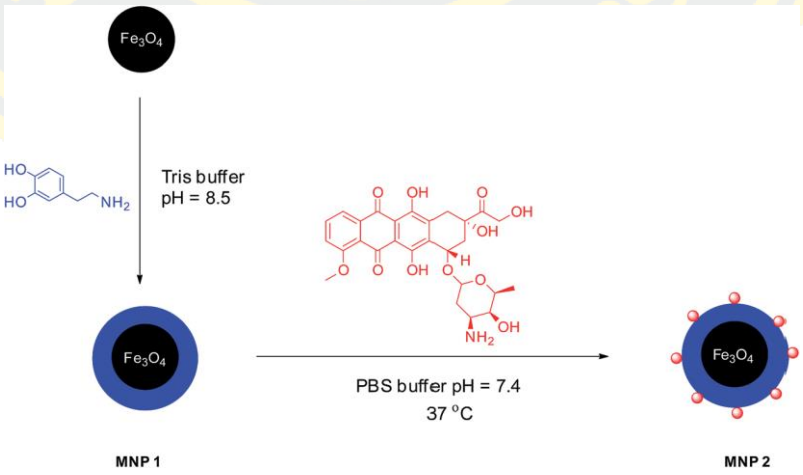

Figure 2-6 The synthesis of magnetic nanoparticles covered with PDA and loaded with doxorubicin (red molecule) (Mrówczyński et al., 2016).

In 2018, Oroujeni, M., et al. demonstrated that magnetic nanoparticles' surface could be functionalized with PDA for immobilizing β-CD ligands. The Fe_3O_4 nanoparticles were coated with polydopamine by oxidation polymerization of dopamine monomer to produce quinone groups. The addition of 6-thio-β-CD to the quinoid structure of polydopamine via a Michael-type addition reaction led to the covalent attachment of the thiol ligands.

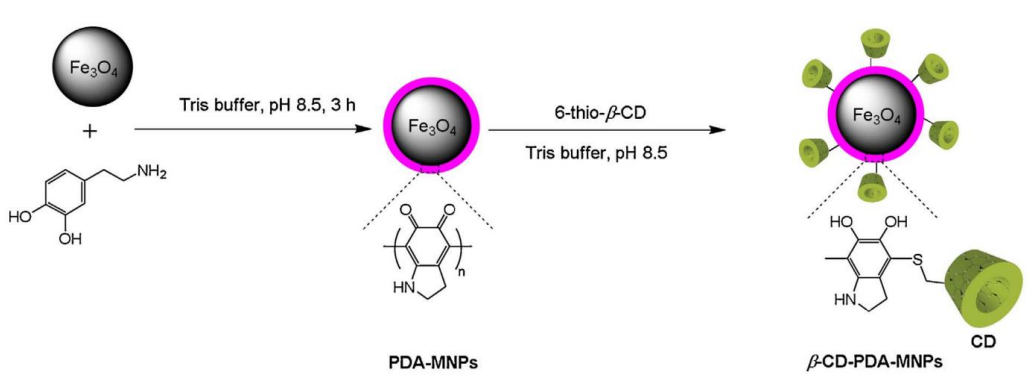

Figure 2-7 Reaction steps for the preparation of β-CD-functionalized magnetic nanoparticles (β-CD-PDA-MNPs)
(Oroujeni, Kaboudin, Xia, Jönsson, & Ossipov, 2018).

2.5 Literature review of iron (III) oxide nanoparticles for bacteria separation

In 2016, Augustine, R. et al. showed that biomolecules such as antibodies, carbohydrates, antibiotics, and binding proteins that are specific to pathogens can be conjugated with IONPs. These IONPs can then be utilized to quickly separate microbes by taking advantage of ligand-receptor interactions. The IONPs are combined with appropriate bacterial ligands or functional groups that have a high affinity for the bacteria, creating a link between the two. Under an external magnetic field, magnetic dipole interactions between the nanoparticles cause them to aggregate, leading to the binding of bacteria to the IONPs and the formation of bacterium nanoconjugates. This causes them to move towards the magnetic field, as illustrated in Figure 2-8. The magnetically attached bacterium nanoconjugates can be removed and decontaminated using suitable sterilization techniques.

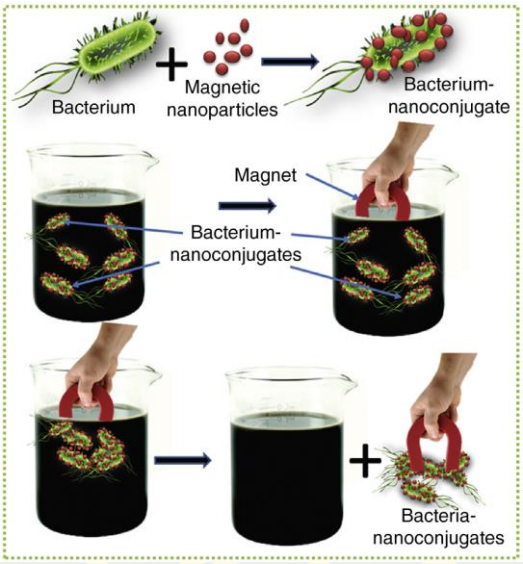

Figure 2-8 The magnetic nanoparticle-based separation of bacteria from a contaminated solution (Augustine, Abraham, Kalarikkal, & Thomas, 2016).

In 2016, Fang, W., et al. Presented the use of two types of amine-functionalized IONPs to produce IONPs capable of effectively capturing pathogenic bacteria. The amine-functionalized IONPs possess a positively charged surface that interacts strongly with the negatively charged bacterial cell wall through electrostatic attraction, indicating their powerful adsorption capability for pathogenic bacteria in circulation. The study showed that Fe_3O_4@sSiO_2-PEI (PEI-MNPs) nanoparticles have three times higher bacteria-binding capability than Fe_3O_4@sSiO_2-NH_2 (NH-MNPs) nanoparticles, making them a promising solution for practical applications as depicted in Figure 2-9.

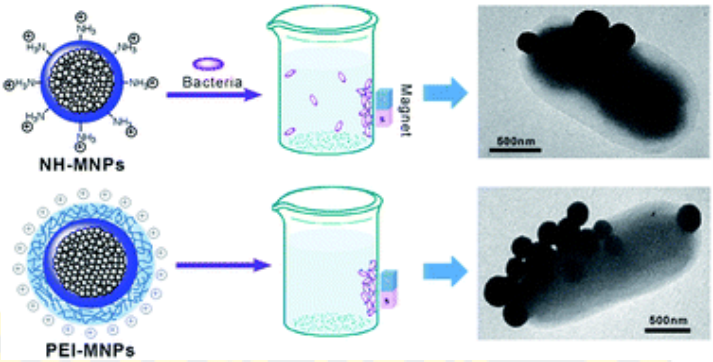

Figure 2-9 Schematic representation of Fe_3O_4@sSiO_2-PEI (PEI-MNPs) nanoparticles modification and Fe_3O_4@sSiO_2-NH_2 (NH-MNPs) nanoparticles catch pathogenic bacteria (Fang et al., 2016).

In 2019, Li et al. In this research, demonstrated a general procedure for capturing bacteria with IONPs. This involved mixing the positively charged (NP^+) and the negatively charged (NP^-) nanoparticles with a bacterial solution, followed by incubation at room temperature. The resulting magnetized bacteria, formed through the binding of magnetic nanoparticles to the cell surface, were captured and separated using a permanent magnet, as shown in the schematic in Figure 2-10. The use of NP^+ provided sufficient electrostatic responsiveness for the rapid enrichment of *E. coli*, whereas the NP^- did not allow for bacteria removal.

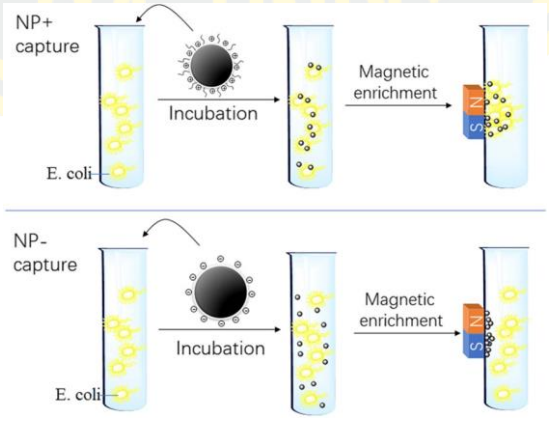

Figure 2-10 Illustration depicts the steps involved in the capture of bacteria with NP^+ and NP^- (Z. Li et al., 2019).

In 2022, Zhang, Y., et al. In this research, employed Fe_3O_4@PDA@PEI magnetic beads to concentrate *E. coli* and *Bacillus subtilis*. The results showed that the MBs-bacterial conjugate method was effective in capturing and enriching the bacteria, enabling efficient separation and reuse of the sample. The captured bacteria were then detected using the ATP-BL method. The results showed that the enrichment with MBs could significantly enhance the ATP fluorescence detection effect.

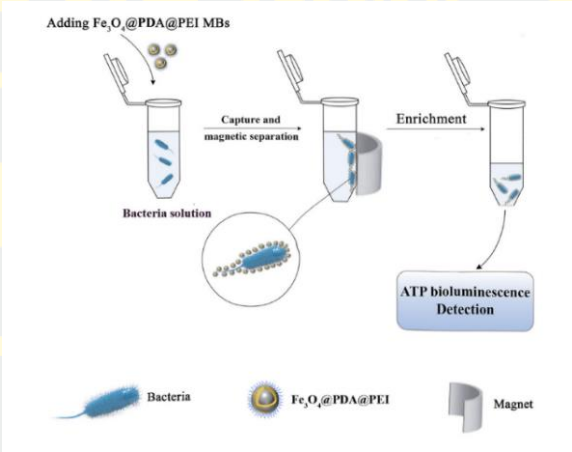

Figure 2-11 Schematic representation of enrichment and detection of bacteria using Fe_3O_4@PDA@PEI MBs (Zhang et al., 2022).

2.6 Detection of bacteria using PGM-based method.

PGM is widely available in the market and used to help patients measure their blood glucose concentrations due to its compact size, low cost, simple operation, and reliable quantitative results. Although the original purpose of PGM is to measure the concentration of glucose in blood, much research has demonstrated that it can be used to detect a broad range of targets, including organic molecules, proteins, and bacteria, etc. The glucose generated in the reaction can be quantified using PGMs, which can then be associated with the concentration of the target. PGM and magnetic nanoparticles (MNPs) have been extensively utilized for the detection of bacteria. Specifically, magnetic particles have been employed for their efficiency in isolating and purifying bacteria from complex biological samples. The isolated bacteria were then detected using PGM, wherein invertases, a group of enzymes that catalyze the hydrolysis of sucrose to produce glucose, were utilized. The glucose concentration

was detected through PGM, and the concentration of bacteria was ultimately determined.

In 2013, Joo, J., et al. developed the detection of *Salmonella* bacteria in milk using a glucose meter (PGM) and monoclonal antibody functionalized MNPs (MNCs). The MNCs were used to capture *Salmonella* bacteria in milk and MNC–Salmonella complexes were magnetically separated from the sample using a permanent magnet. Subsequently, the complex was linked with the functional invertase of a polyclonal antibody, which facilitated the hydrolysis of sucrose to glucose. The glucose was then quantified using PGM, as shown in the schematic in Figure 2-12.

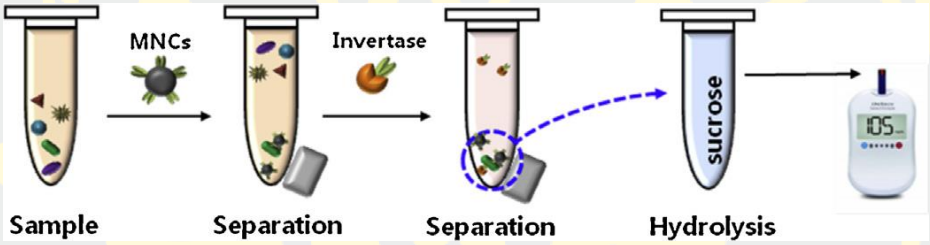

Figure 2-12 Schematic of the detection of *Salmonella* bacteria experimental procedure using a PGM (Joo et al., 2013).

As an alternative approach, since bacteria prefer glucose as their carbon source, the hypothesis is that the bacteria can consume the glucose, and the resulting change in glucose concentration can be monitored using a PGM.

In 2014, Chavali, R., et al. demonstrated the detection of *E. coli* in drinking water using PGM-based method. The detection of *E. coli* was achieved by monitoring the consumption of glucose by *E. coli*. The result showed that the drop in glucose levels for certain concentrations of *E. coli* is presented shown in Figure 2-13. However, this method still falls short in complying with the regulations of environmental protection agencies, which require a volume of 100 mL for testing water samples.

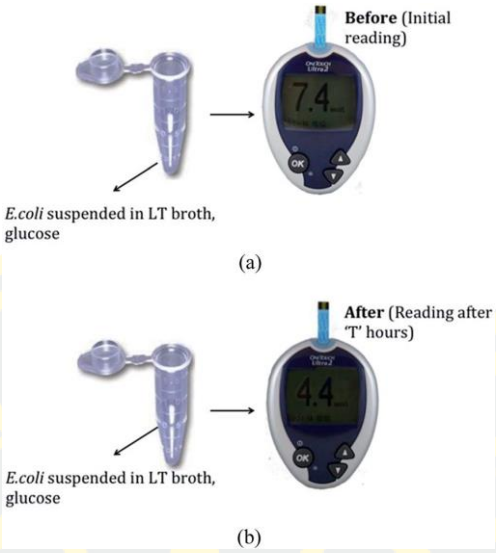

Figure 2-13 Schematic representation of the detection process: (a) Initial readings of the mixture taken immediately after the addition of glucose (T = 0 h) (b) readings taken after 'T' hours depending on the level of contamination of the water samples (Chavali, Kumar Gunda, Naicker, & Mitra, 2014).

In 2017, Ye, L., et al. introduced a new technique for detecting *C. sakazakii* using a personal glucose meter (PGM) as the readout, which is low-cost, simple, and widely available. The detection method involved using silica nanoparticles coated with antibodies and glucose oxidase (SiNP-GOX-IgG) and silica-coated magnetic nanoparticles functionalized with antibodies (MNP-IgG). The MNP-IgG was used to isolate *C. sakazakii* from the samples while the SiNP-GOX-IgG was used as a trace tag for detection, where glucose would be hydrolyzed. The concentration change of glucose was measured using a commercial PGM.

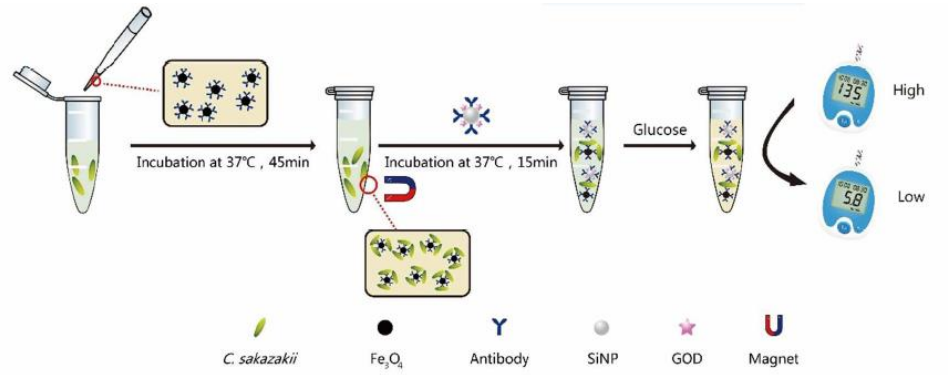

Figure 2-14 Schematic of the detection procedure for *C. sakazakii* using SiNP-GOX-IgG, MNP-IgG typical sandwich feature and PGM (Ye, Zhao, & Dou, 2017) .

In 2018, Kwona, D., et al. utilized the idea of glucose being consumed by bacterial metabolism to detect enrofloxacin in water and milk. The detection procedure involved mixing the test sample with *Escherichia coli (E. coli)* in lysogeny broth (LB) and glucose. The amount of glucose consumed by bacterial metabolism was measured using PGM, resulting in a sensitive, quantitative, and portable detection method. Moreover, the change in glucose concentration could be determined qualitatively by the naked eye using glucose test strips, allowing for high-throughput screening.

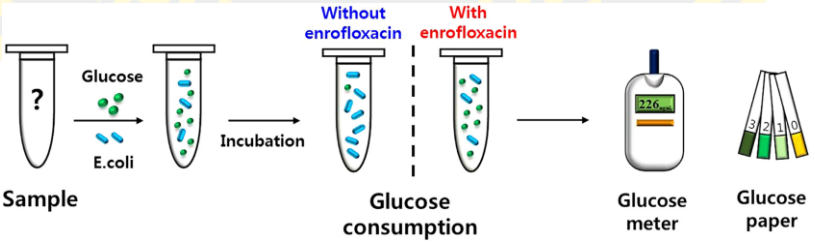

Figure 2-15 The process of enrofloxacin detection in a test sample solution containing glucose and *E. coli*, using either a personal glucose meter or glucose paper test strips (Kwon et al., 2018).

CHAPTER 3
EXPERIMENTALS

3.1 Materials

1. 28%w/v Ammonia solution; NH_3OH, MW: 35.05 g/mol, CAS: 1336-21-6 (QREC, New Zealand)
2. Iron (II) chloride tetrahydrate; $FeCl_2 \cdot 4H_2O$, MW: 198.81 g/mol, CAS: 13478-10-9 (Sigma-Aldrich, USA)
3. Iron (III) chloride tetrahydrate; $FeCl_3 \cdot 6H_2O$, MW: 270.30 g/mol, CAS: 13478-10-9 (Sigma-Aldrich, USA)
4. Phosphate buffer saline; PBS (Sigma-Aldrich, USA)
5. Dopamine hydrochloride; $(HO)_2C_8H_7NH_2 \cdot HCl$, MW: 189.64 g/mol, CAS: 62-31-7 (Sigma-Aldrich, USA)
6. Tris (hydroxymethyl) aminomethane; $NH_2C(CH_2OH)_3$ (Tris-HCl), MW: 121.14 g/mol, CAS: 77-86-1 (OmniPur®, Germany)
7. Chitosan (poly-D-glucosamine), medium molecular weight, CAS: 9012-76-4 (Sigma-Aldrich, USA)
8. Acetic acid; CH_3COOH, MW: 60.05 g/mol CAS: 64-19-7 (QReC™, New Zealand)
9. D(+)-Glucose anhydrous; $C_6H_{12}O_6$, MW: 180.66g/mol CAS: 50-99-7 (KemAus, Australia)
10. Luria Bertani Broth, Miller, CAS: M1245 (Himedia™ / India)
11. Sodium chloride 99.5%; NaCl, MW: 58.44g/mol CAS: 7647-14-5 (MERCK™, Germany)
12. Citric Acid Anhydrous 99.5%; $C_6H_8O_7$, MW: 192.13g/mol CAS: 77-92-9 (QReC™, New Zealand)

3.2 Bacteria and culture conditions

1. *Escherichia coli* (*E. coli*) ATCC25922 was supported by Dr. Yothin Teethasong from the Faculty of Allied Health Sciences, Burapha University
2. *Staphylococcus aureus* (*S. aures*) ATCC29213 was provided by Dr. Yothin Teethasong from the Faculty of Allied Health Sciences, Burapha University

3.3 Instrument

1. pH meter
2. Oven, model OF-01E
3. Micropipette, model Research plus, Eppendorf
4. Ultrasonic bath, model ELMA S30H
5. Vortex shaker, model Vortex-Genie 2 Shaker
6. Glass reactor (500 mL), Schott Duran
7. Hotplate with stirrer, model C-MAGHS7, IKA
8. Mechanical stirrer, model RW 20 digitals, IKA
9. Balance, model ML204/01, Mettler Toledo
10. Atten Attenuated Total Reflectance Fourier Transform Infrared Spectrometer (ATR-FTIR), PerkinElmer -Frontier
11. Transmission electron microscopy (TEM), Philips Tecnai 20
12. Scanning Electron Microscope (SEM), LEO 1450 VP
13. Zetasizer Nano-ZS, Malvern 3600
14. Portable glucose meters (PGMs), Accu-Chek Active
15. Spectrophotometric, Analytikjena, Specord 210 plus, Germany
16. Microplate reader, SpectraMAX M2, Molecular Devices

3.4 Experimental section

3.4.1 Synthesis of magnetite nanoparticle (MNPs)

Magnetite nanoparticles (MNPs) were prepared by the chemical co-precipitation method, in accordance with previously published literature (Sadsri, V., Trakulsujaritchok, T., Tangwattanachuleeporn, M., Hoven, V. P., & Na Nongkhai, P., 2020). A solution of ferric and ferrous salts was prepared by dissolving $FeCl_3 \cdot 6H_2O$ (1M, 1.7880g) and $FeCl_2 \cdot 4H_2O$ (2M, 0.6840g) in 60 mL of deionized water, followed by sonication for 10 minutes. Subsequently, the mixed solution was added to a three-neck flask under a N_2 gas atmosphere, and the flask was heated to 60°C with high-speed stirring (750 rpm) for 30 minutes. A total of 36 mL of 28% (w/v) ammonia solution was slowly added to the solution, and the mixture was stirred for 2 hours. During this process, the color of the solution changed from yellow orange to black, indicating the formation of magnetite nanoparticles (MNPs). In order to stabilize the MNPs, citric acid (0.1M) was added and allowed to react for 1 hour. The mixture was then cooled down to room temperature. The citric stabilized-MNPs were thoroughly washed multiple times with deionized water to eliminate any remaining unreacted chemicals, continuing until a neutral pH was achieved. The citric stabilized-MNPs were then redispersed in deionized water and stored at room temperature until they were used.

$$Fe^{2+}(aq) + 2Fe^{3+}(aq) + 8OH^{-}(aq) \longrightarrow Fe_3O_4(s) + 4H_2O \quad (1)$$

3.4.2 For electrostatic adsorption

3.4.2.1 Preparation of Chitosan modified MNPs (MNPs-CH)

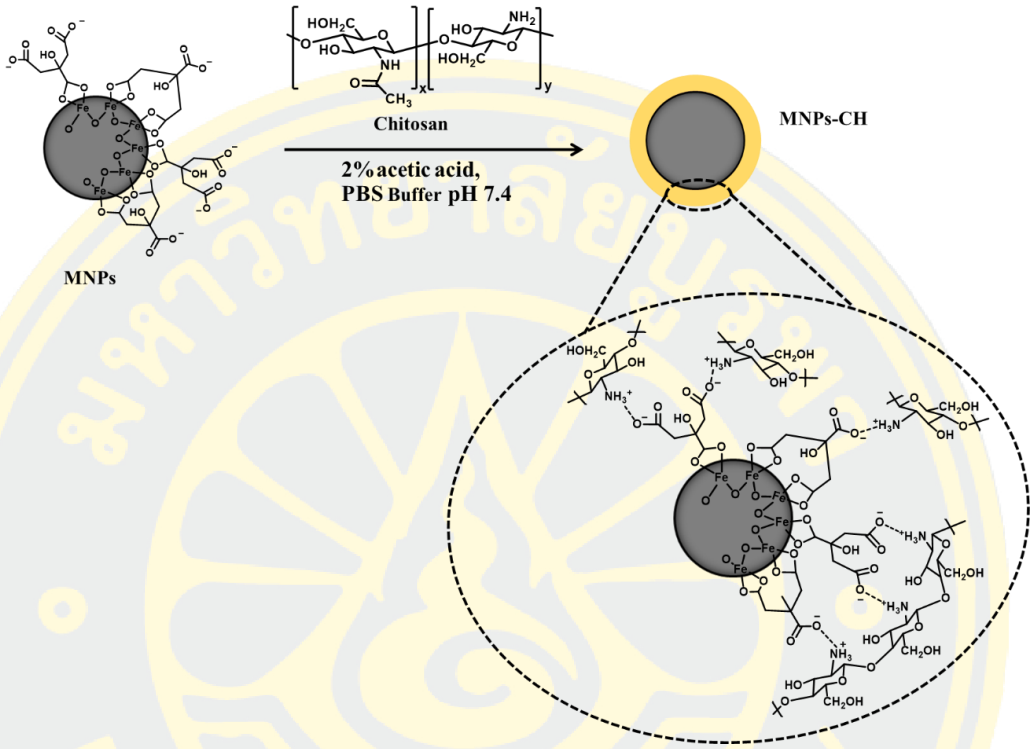

Chitosan modified MNPs were prepared with electrostatic interaction between the positively charged chitosan and the negatively charged citric stabilized MNPs. The 100 mg of obtained citric stabilized-MNPs from section 3.3.1 was washed with PBS buffer (20 mM, pH 7.4) and redispersed in 20 mL of PBS buffer (20 mM, pH 7.4). The chitosan solution was prepared by dissolving chitosan with different amounts (12.5, 25, and 50 mg) in 20 mL of 2% acetic acid and stirred overnight at room temperature. The chitosan solutions were added to the mixture MNPs dispersion and agitated with shaker at 300 rpm for 4, 8, and 16 hours. The resulting MNPs-CH were washed with deionized (DI) water and separated from the solution using a magnet. Finally, the MNPs-CH were resuspended in DI water and stored at room temperature.

3.4.3 For covalent adsorption

3.4.3.1 Synthesis of polydopamine coated MNPs (MNPs-PDA)

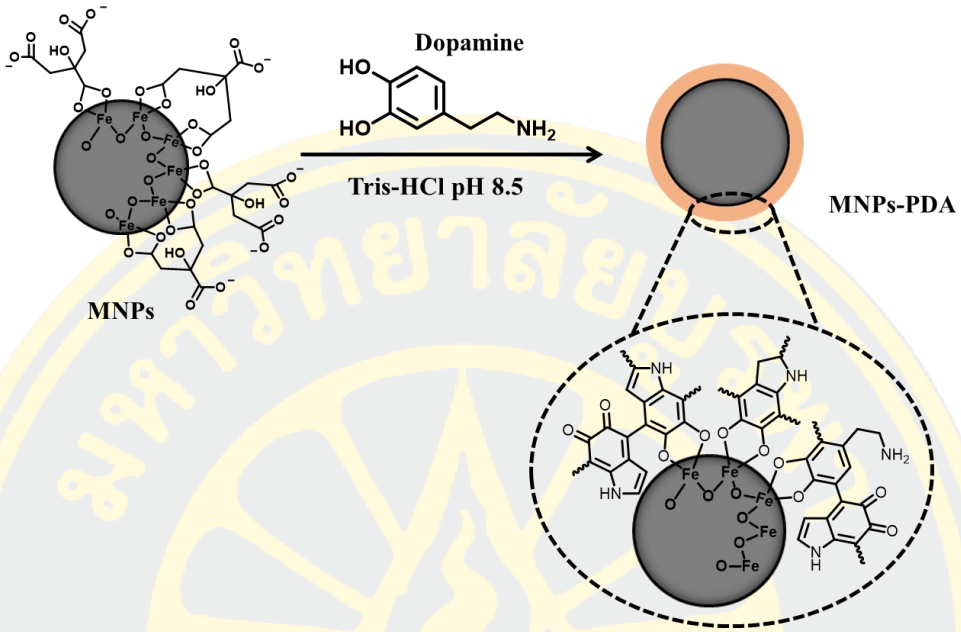

The MNPs were modified with dopamine using the following procedure: First, 125 mg of citric stabilized-MNPs were washed with Tris-HCl buffer solution (50 mM, pH 8.5) for 2-3 cycles. Then, 20 mg of dopamine monomer was dissolved in 10 mL of Tris-HCl buffer and added to the citric stabilized-MNPs. The reaction was incubated at room temperature with constant shaking conditions for 1, 4, 8, 16 and 24 hours. The products were then washed with distilled water for 5 cycles. The MNPs-PDA were then redispersed in deionized water and stored at room temperature until they were used.

3.4.3.2 Preparation of Chitosan modified MNPs-PDA (MNPs-PDA-CH)

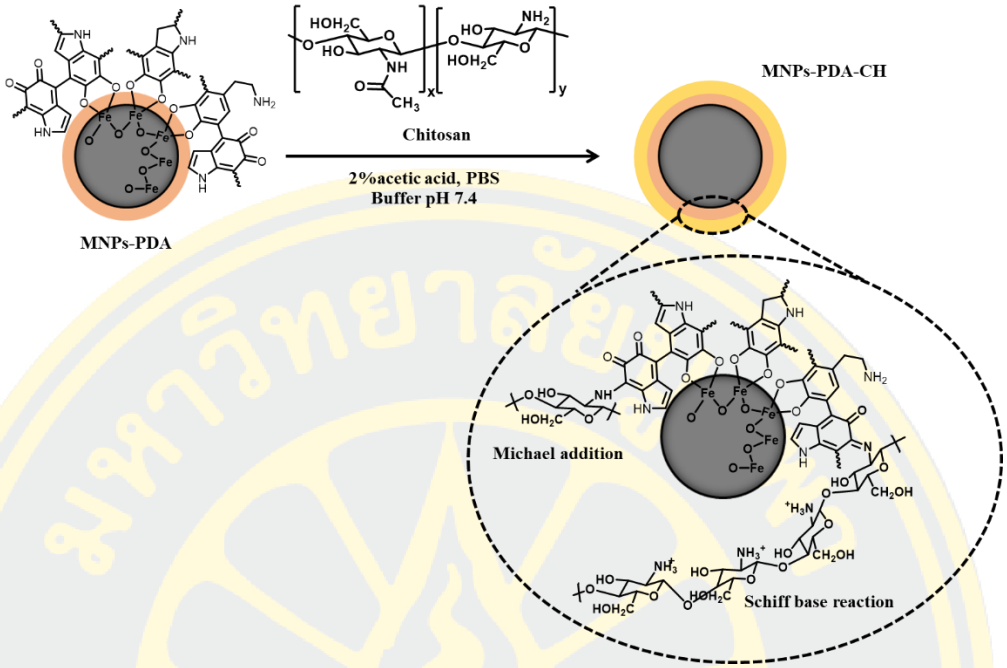

Chitosan modified MNPs-PDA were prepared with covalent bond between the quinone group of PDA and the amino groups of chitosan via Shift based reaction and Michael addition. The 100 mg of obtained MNPs-PDA from section 3.3.2 was washed with PBS buffer (20 mM, pH 7.4) and redispersed in 20 mL of PBS buffer (20 mM, pH 7.4). The chitosan solution was prepared by dissolving chitosan with different amounts (12.5, 25, and 50 mg) in 20 mL of 2% acetic acid and stirred overnight at room temperature. The chitosan solutions were added to the mixture MNPs-PDA dispersion and agitated with shaker at 300 rpm for 4, 8, and 16 hours. The resulting MNPs-PDA-CH were washed with deionized (DI) water and separated from the solution using a magnet. Finally, the MNPs-PDA-CH were resuspended in DI water and stored at room temperature.

3.4.4 Examination of bacterial separation

3.4.4.1 Bacterial culture

The *E. coli* and *S. aures* bacteria were cultured in Nutrient Broth medium at 37°C for 16 h. The optical density (OD) was measured by a UV spectrometer to estimate bacterial concentration. Each experiment was conducted using fresh *E. coli* and *S. aures* at OD = 2.0 at a wavelength of 600 nm.

3.4.4.2 Separation of bacteria with MNPs-PDA-CH and MNPs-CH

E. coli (Gram-negative bacteria) and *S. aures* (Gram-positive bacteria bacteria) were selected in this experiment 1.0 mL of bacterial suspension in PBS buffer pH 5.0 and 7.4 (OD = 2.0) was mixed with magnetic nanoparticles 1 mg of MNPs-PDA-CH and MNPs-CH and incubated at room temperature for 30 minutes under gentle shaking. When the designated time elapses, the particles are separated from the solution using a strong magnetic field. The separated solution was then measured for OD at a wavelength of 600 nm. Calculate the %Bacteria capture value from equation 2.

$$\% \text{ Bacteria capture} = \frac{C_0 - C_e}{C_0} \times 100 \qquad (2)$$

C_0 is the OD of bacteria suspension before capturing

C_e is the OD of bacteria suspension after capturing

3.4.5 Detection of bacteria using magnetic nanoparticles in combination with a glucometer

3.4.5.1 Preparation of Escherichia coli ATCC 25922

E. coli was transferred from glycerol into stock Luria-Bertani (LB) Broth and subsequently incubated at 37 °C for 24 hours to increase the number of bacteria. The cells were centrifuged at 10,000 rpm for 10 minutes, after which the supernatant was removed, and the cells were washed once with PBS buffer (10 mM, pH 5.0). Afterwards, the cells were carefully transferred into a test tube and adjusted until the turbidity reached a McFarland value of 0.5.

3.4.5.2 Preparation of Staphylococcus aureus ATCC 29213

S.aureus was cultured from glycerol stock into Luria-Bertani (LB) Broth and subsequently incubated at 37 °C for 24 hours to increase the number of bacteria. The cells were centrifuged at 10,000 rpm for 10 minutes, after which the supernatant was removed, and the cells were washed once with PBS buffer (10 mM, pH 5.0). Afterwards, the cells were carefully transferred into a test tube and adjusted until the turbidity reached a McFarland value of 0.5.

3.4.5.3 Detection procedure

The captured bacteria were detected using portable glucose meters (PGMs) based on the concept of monitoring the glucose consumption by bacteria. If bacteria are present in the sample, they will consume glucose, resulting in a detectable change in glucose concentration that can be measured by the PGM. The captured bacteria were detected using portable glucose meters (PGMs) based on the concept of monitoring the glucose consumption by bacteria. If bacteria are present in the sample, they will consume glucose, resulting in a detectable change in glucose concentration that can be measured by the PGM. The 5.0 mL of bacterial samples (McFarland = 0.5, ~1.5×10^8 CFU/mL) was mixed with chitosan modified-MNPs and incubated at room temperature under gentle shaking for 30 minutes. The chitosan modified-MNPs-bacteria complex was separated magnetically, and the clear supernatant was discarded. The complex was then washed with PBS to remove unbound bacteria. Then 100 µL of Luria-Bertani broth (LB) and 1%w/v glucose were added to 10 µL. The mixture was incubated with shaking at 37 °C. The solution was dropped onto the PGM strip, and the glucose concentration was gauged by tracking the variation in glucose levels within the solution at various intervals. Compared to conditions without bacteria (control), calculate the percentage of glucose consumption (%ΔC) from the equation 3.

$$\%\Delta C = \frac{(C_0 - C_e)}{C_0} \times 100 \quad (3)$$

C_0 is the initial concentration of glucose in the reaction solution (mg/dL)

C_e is the remaining concentration of glucose in the reaction solution at a specific time interval (mg/dL)

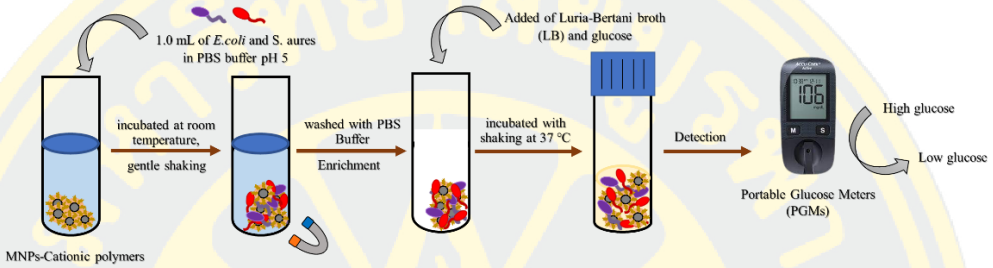

Figure 3-1 Illustrates the steps in measuring bacteria using a glucose meter.

3.4.6 Detection of bacteria in dried seafood

Dried shrimp and dried squid were purchased from Nong Mon Market in Chonburi, Thailand. Ten grams of the dried samples were soaked in 10 mL of PBS buffer (10 mM, pH 5.0). The solution of the sample was detected by plate culture method. The same sample solution was also analyzed using our method with procedures similar to those described above.

CHAPTER 4
RESULTS AND DISCUSSION

4.1 Synthesis of magnetic nanoparticle (MNPs)

Magnetic nanoparticles were synthesized using the co-precipitation method of two types of iron ions, Fe^{2+} and Fe^{3+}, under a nitrogen atmosphere and using ammonium hydroxide (NH_4OH, 28%) as a precipitating agent. The stability of the magnetic nanoparticles was then stabilized with citric acid. The reaction equation of MNPs is as follows:

$$Fe^{2+}(aq) + 2Fe^{3+}(aq) + 8OH^{-}(aq) \longrightarrow Fe_3O_4(s) + 4H_2O(l) \quad (2)$$

ATR-FTIR spectrum of MNPs showed a characteristic absorption peak located at 539 cm^{-1} which belongs to Fe-O bond in MNPs. Moreover, the absorption peak located at 1597 cm^{-1} and 1370 cm^{-1} are formed by the asymmetric and symmetric C-O stretching of COO^- group in citric acid, respectively (Figure 4-1). The TEM image shows the morphology and size of MNPs. It was shown that the MNPs had a spherical shape and range approximately in size of 15-20 nm (Figure 4-2). The obtained MNPs exhibited magnetic properties, allowing them to be readily separated from the solution by induction using an external magnetic field within 40 seconds (Figure 4-3). From the results of the analysis of the composition and quantity of elements on the MNPs using the Energy Dispersive X-ray spectroscopy (EDX) technique, it was found that the MNPs consisted of the elements Fe (42.48% At) and O (38.28% At), corresponding to the iron oxide nanoparticles. Moreover, the C elements (19.24%At) from citric acid were also detected, confirming the successful stabilization of MNPs by citric acid.

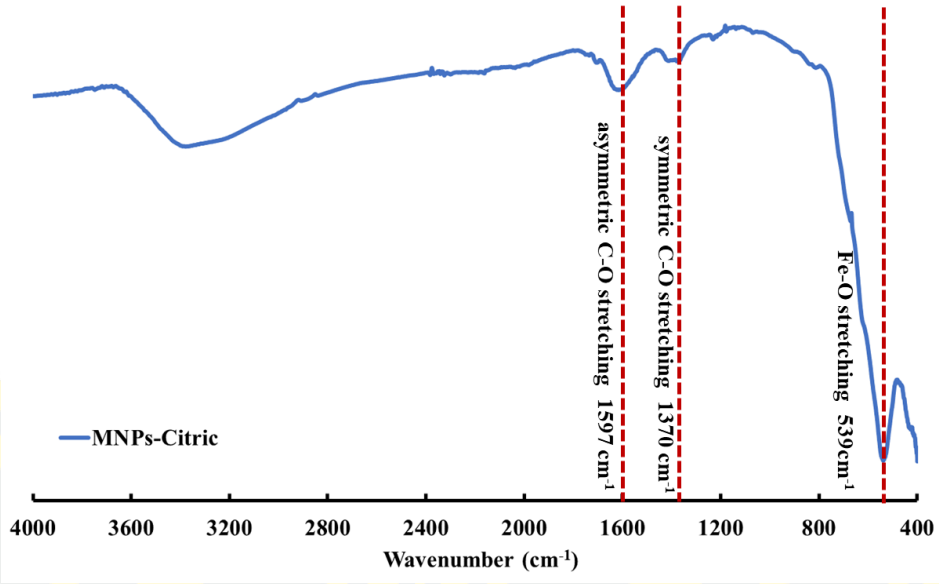

Figure 4-1 ATR-FTIR spectra of citric-stabilized MNPs.

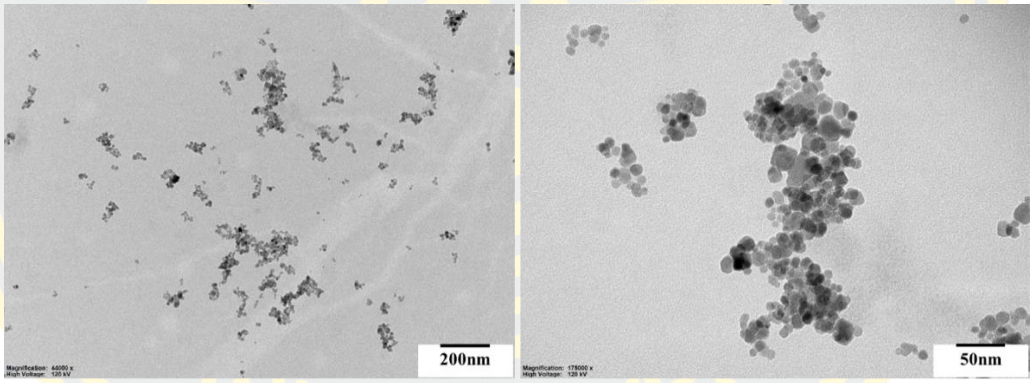

Figure 4-2 TEM image of MNPs-Citric

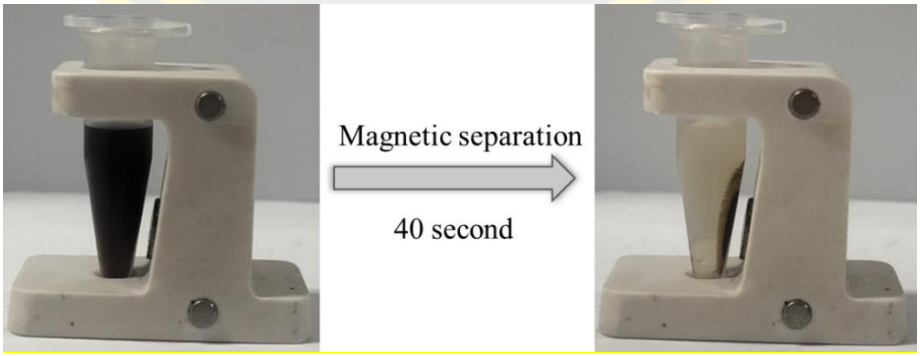

Figure 4-3 Magnetic properties image of MNPs-Citric

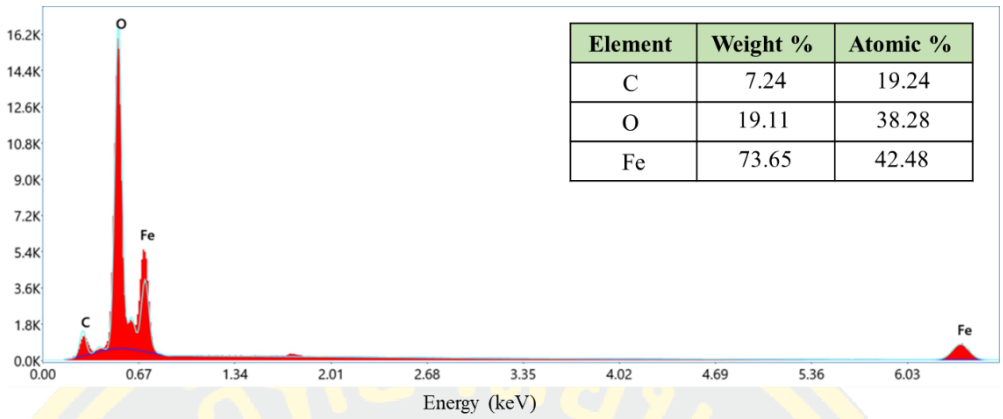

Element	Weight %	Atomic %
C	7.24	19.24
O	19.11	38.28
Fe	73.65	42.48

Figure 4-4 EDX analysis of MNPs-Citric

4.2 Preparation of Chitosan modified MNPs (MNPs-CH) via electrostatic adsorption method

To enhance the positive charge of the MNPs surface, The MNPs were then modified with chitosan. This modification was achieved through electrostatic interaction between the negative charged citric acid and the positive charge of chitosan (Figure 4-5).

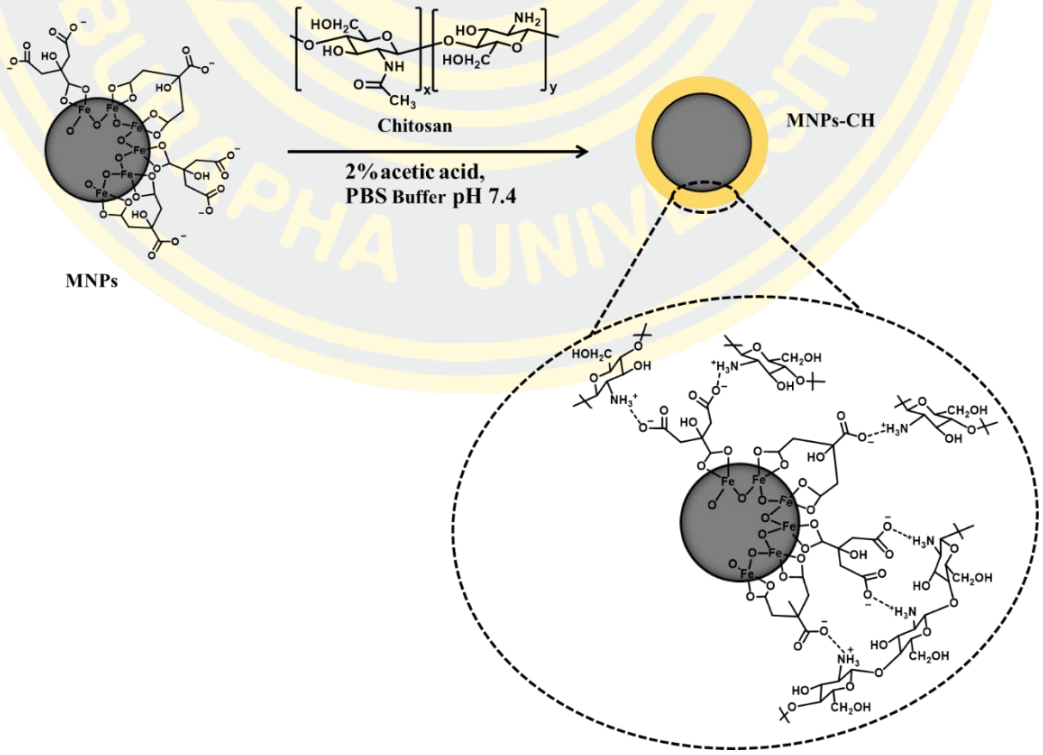

Figure 4-5 Illustrates the preparation of chitosan-modified MNPs (MNPs-CH)

ATR-FTIR spectrum of MNPs-CH (Figure 4-6) with various concentrations of chitosan demonstrated the characteristic absorption peak located at 539 cm^{-1}, belonging to Fe-O bond in MNPs. The peaks at 1066 cm^{-1} exhibited the characteristic of chitosan corresponding to C-O-C stretching vibration of the polysaccharide. Based on this observation, it can be concluded that chitosan was anchored on the surface of MNPs.

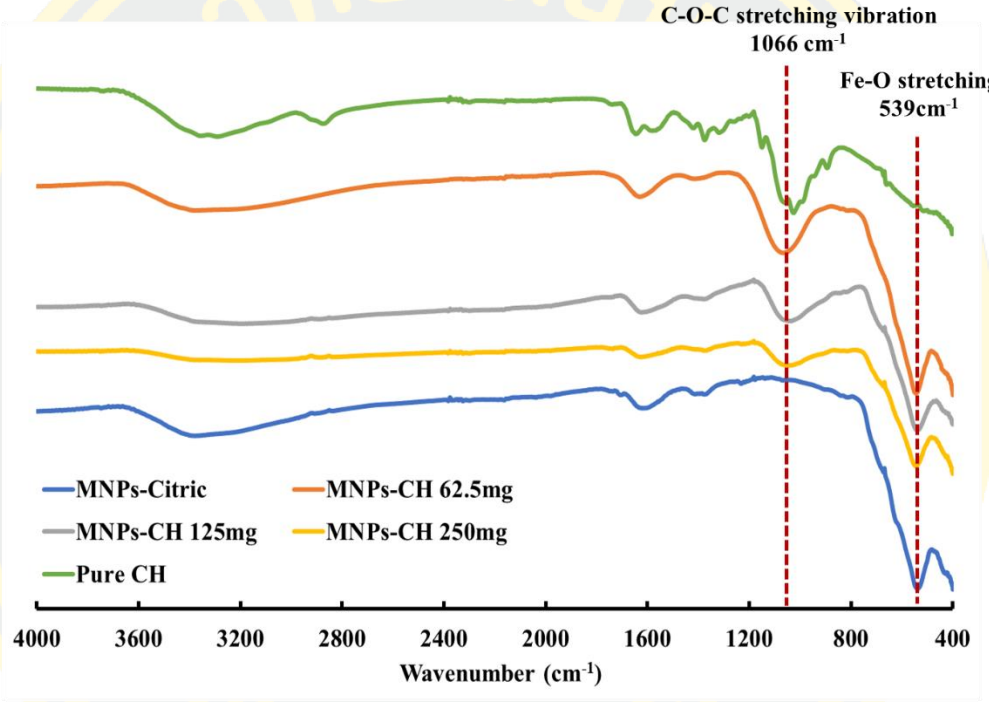

Figure 4-6 ATR-FTIR spectra of MNPs-Citric modified with chitosan

Figure 4-7 shows the TEM images of MNPs-CH with various concentrations of chitosan. It was found that MNPs-CH appeared to form larger clusters of nanoparticles compared to MNPs-citric (Figure 4-2). The hydrodynamic diameter obtained from DLS technique also confirmed the increase of nanoparticles size after chitosan modification corresponding to the TEM images (Figure 4-8).

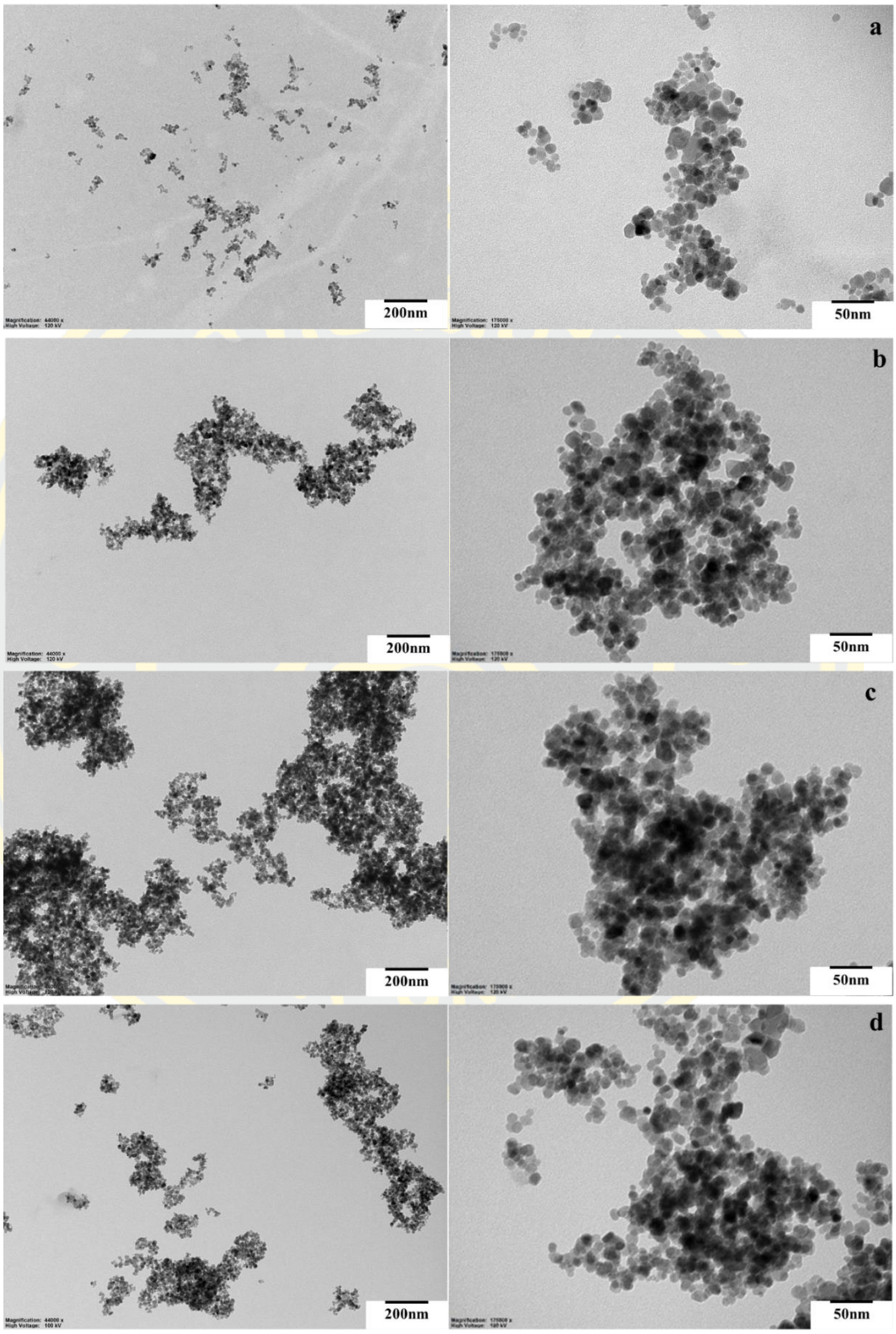

Figure 4-7 TEM image of (a) MNPs-Citric, (b) MNPs-CH 62.5 mg , (c) MNPs-CH 125 mg and (d) MNPs-CH 250 mg

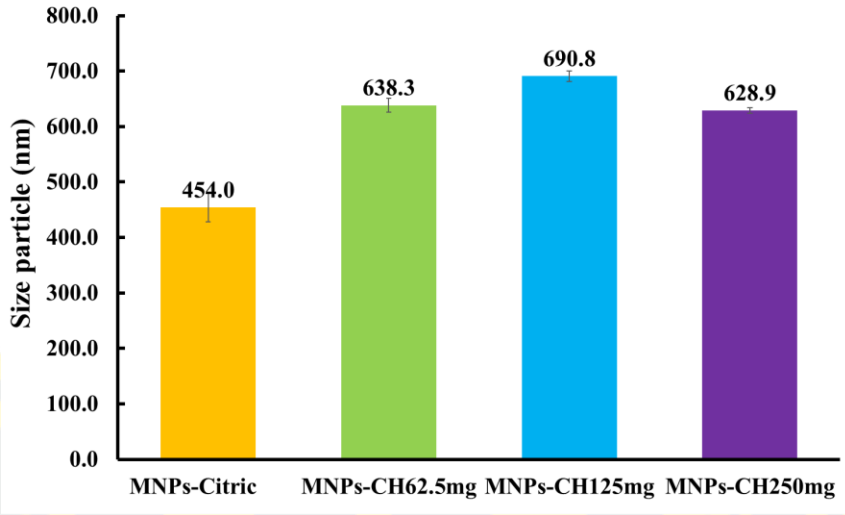

Figure 4-8 Hydrodynamic diameter of MNPs-Citric and MNPs-CH with various concentrations of chitosan. The data were expressed as mean ± SD.

The zeta potential of the MNPs-citric changed from a negative value (-4.7 mV) to a positive value after coating with chitosan (Figure 4-9). This result indicated that the surface of MNPs was successfully covered with positively charged chitosan. When considering the effect of chitosan concentration, it was found that the positive value trended to increase with increasing chitosan concentration from 62.5 to 250 mg. However, when the concentration of chitosan was higher than 125 mg, the positive value did not change significantly.

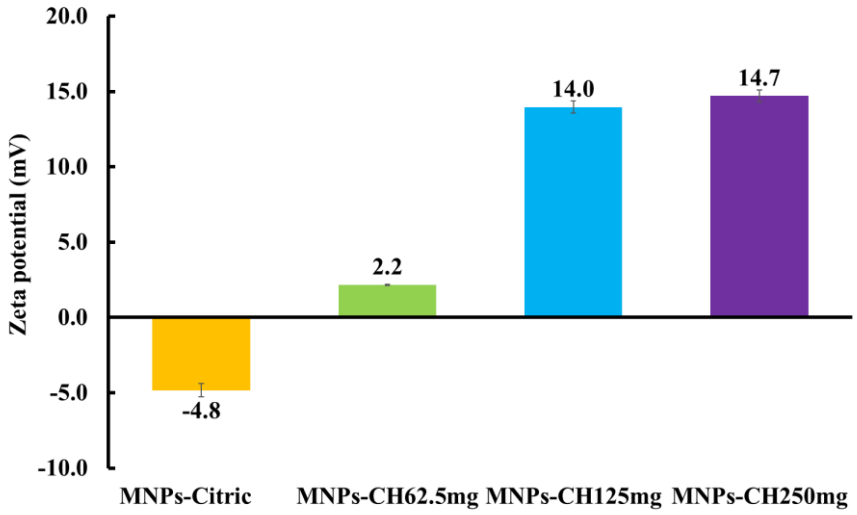

Figure 4-9 Zeta potential analysis of MNPs-Citric and MNPs-CH with various concentrations of chitosan.

Figure 4-10 shows the magnetic properties of MNPs-CH with various concentrations of chitosan, 62.5, 125, and 250 mg, respectively. They were induced using an external magnetic field within 30, 42, and 46 seconds, respectively. This indicates effective and rapid magnetic properties.

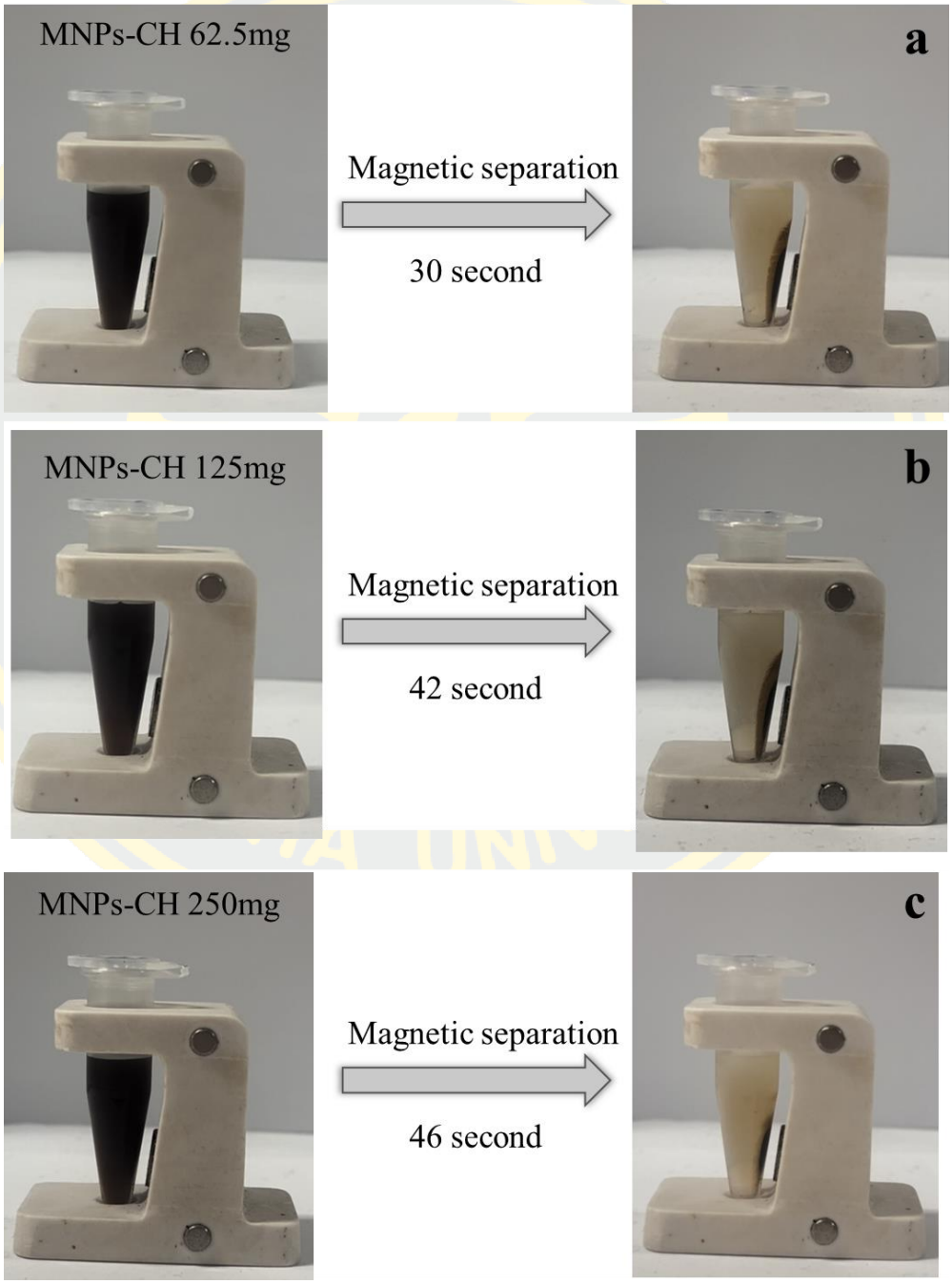

Figure 4-10 Magnetic properties image of (a) MNPs-CH 62.5 mg, (b) MNPs-CH 125 mg and (c) MNPs-CH 250 mg.

4.3 Preparation of Chitosan modified MNPs (MNPs-PDA-CH) via covalent adsorption method

4.3.1 Synthesis of polydopamine coated MNPs (MNPs-PDA)

The MNPs were first modified with polydopamine *via* the oxidative polymerization of dopamine monomer to provide active functional groups, such as quinone, for the covalent anchoring of chitosan on the surface of MNPs (Figure 4-11).

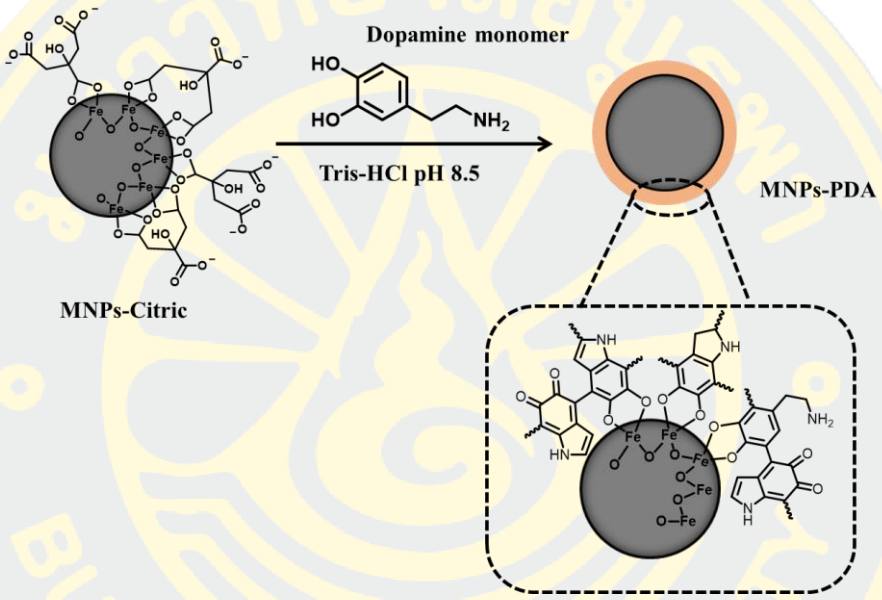

Figure 4-11 Illustrates the preparation of polydopamine-modified MNPs (MNPs-PDA)

Figure 4-12 showed the ATR-FTIR spectrum of MNPs-PDA. The new peaks located at 1284 and 1472 cm^{-1} exhibited the characteristics of PDA corresponding to the stretching vibrations of the C-N and the aromatic C=C, respectively (Lamaoui, 2021). These results indicated that the surface of MNPs has been successfully modified with PDA, enabling the covalent anchoring of chitosan on their surface *via* Shift based reaction and Michael addition in subsequent steps.

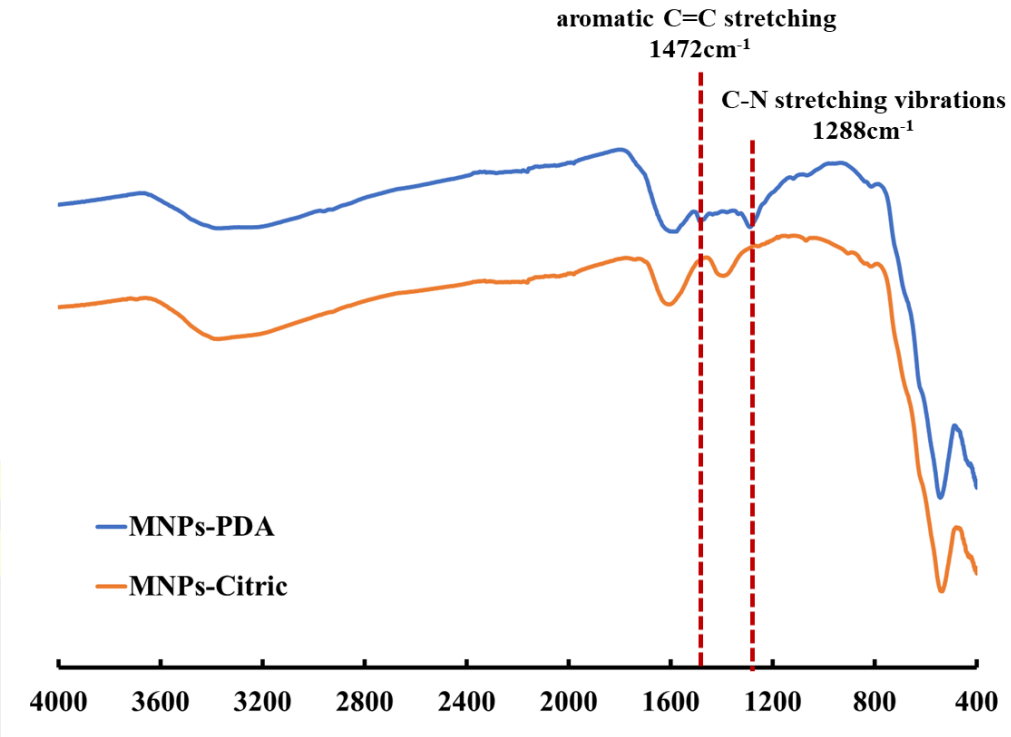

Figure 4-12 ATR-FTIR spectra of MNPs-citric and MNPs-PDA

The effect of polymerization time of dopamine monomer was evaluated. The ATR-FTIR spectrum (Figure 4-13) showed that the intensity of peaks at 1288 and 1472 cm^{-1} increased with increasing polymerization time. This result indicates that the polymerization of dopamine is dependent on the duration of polymerization.

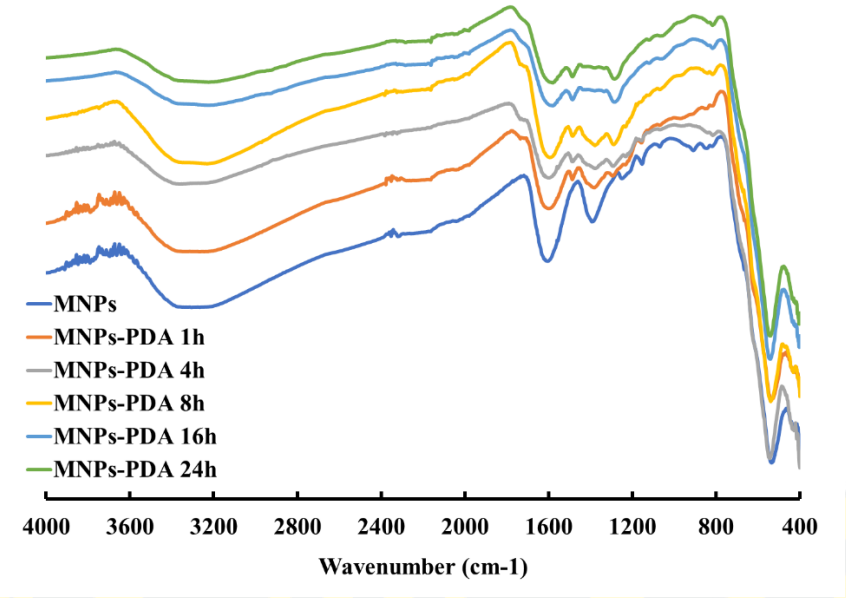

Figure 4-13 ATR-FTIR spectra of polymerization time 1 to 24 hours of dopamine monomer.

The result from zeta potential analysis revealed that the charge value shifted from a negative (-7.1 mV) to a positive value (+9.6 mV) when the polymerization time ranged from 1 to 4 hours (Figure 4-15). This observation suggests that during this time (1-4 h), dopamine monomers are covalently bound to the surface of MNPs through a chelating bidentate interaction of catechol groups with the Fe atom. Consequently, the surface of MNPs primarily comprises amino groups of dopamine. However, prolonged polymerization times (16-24 h) induces a structural transition of dopamine into polydopamine, as evidenced by the zeta potential shift from positive amino groups to negative dihydroxy indole and quinone groups. This result indicated that the suitable polymerization time was longer than 16 h.

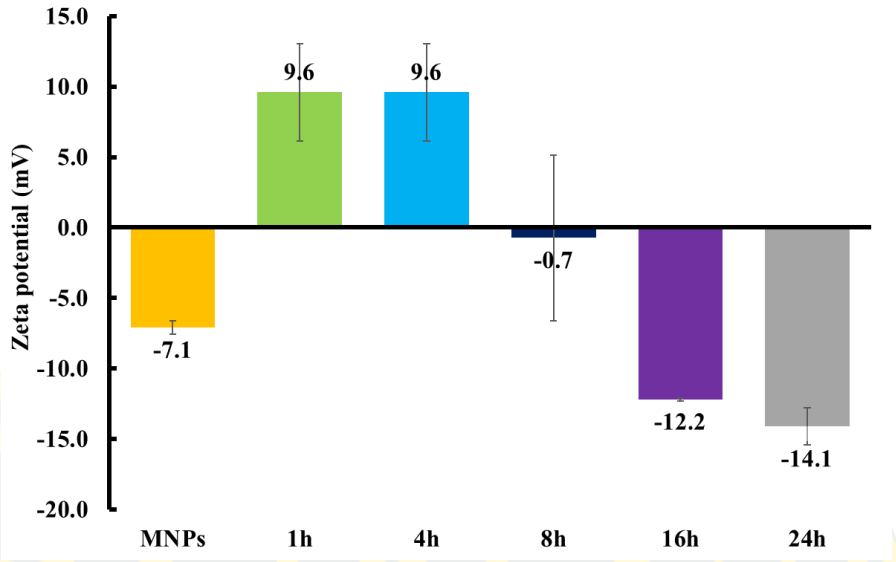

Figure 4-14 Zeta potential of MNPs-PDA with difference polymerization time

Figures 4-15 and 4-16 showed the TEM image and particles size of MNPs-PDA. MNPs-PDA formed clusters of nanoparticles with a cluster size ranging from 200 to 500 nm. Additionally, the hydrodynamic diameter obtained from DLS measurements also indicated that the size of MNPs-PDA ranged from 200 to 300 nm when the polymerization time ranged from 16 to 24 hours.

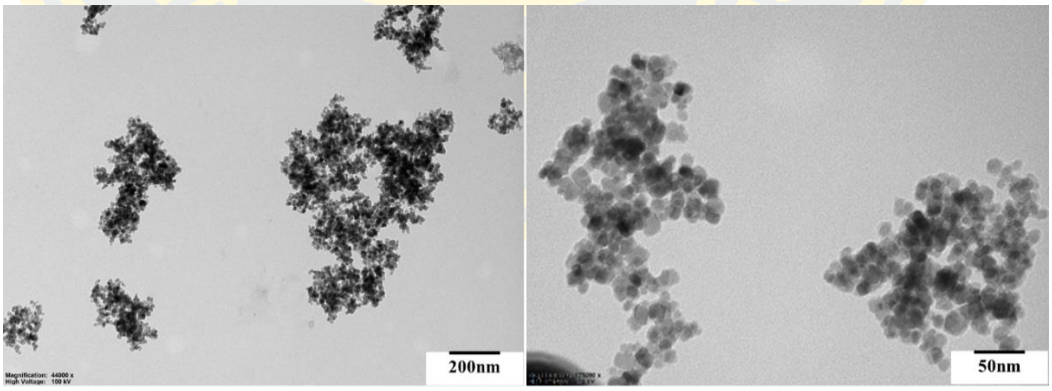

Figure 4-15 TEM image of MNPs-PDA 16 hours

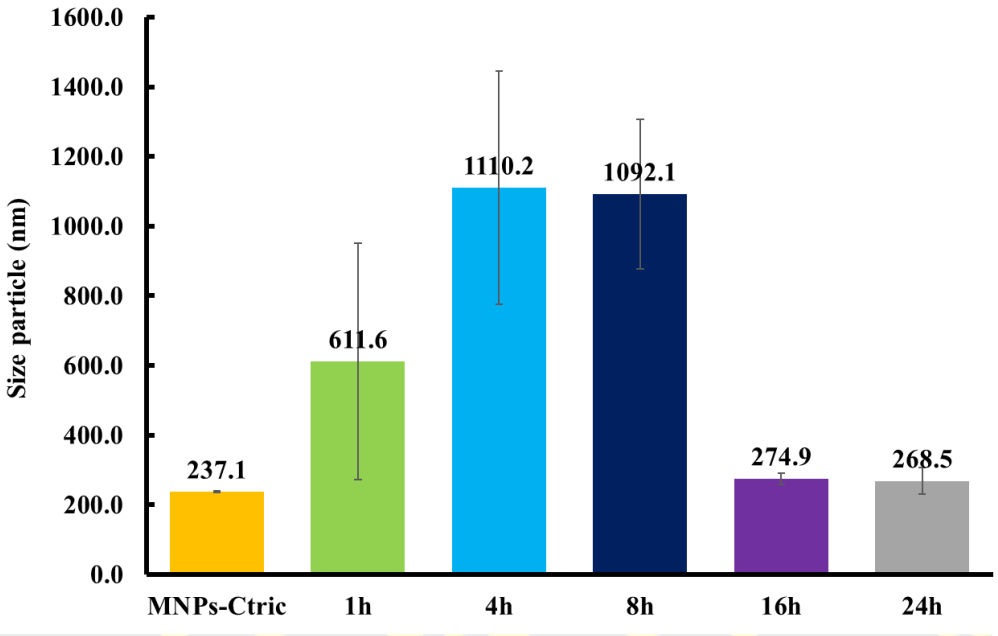

Figure 4-16 Hydrodynamic diameter of MNPs-PDA with difference polymerization time. The data were expressed as mean ± SD

4.3.2 Preparation of Chitosan modified MNPs-PDA (MNPs-PDA-CH)

The MNPs-PDA were subsequently modified with chitosan. This modification was achieved through the formation of a covalent bond between the quinone group of PDA and the amino groups of chitosan *via* a Shift-based reaction and Michael addition, as illustrated in Figure 4-17.

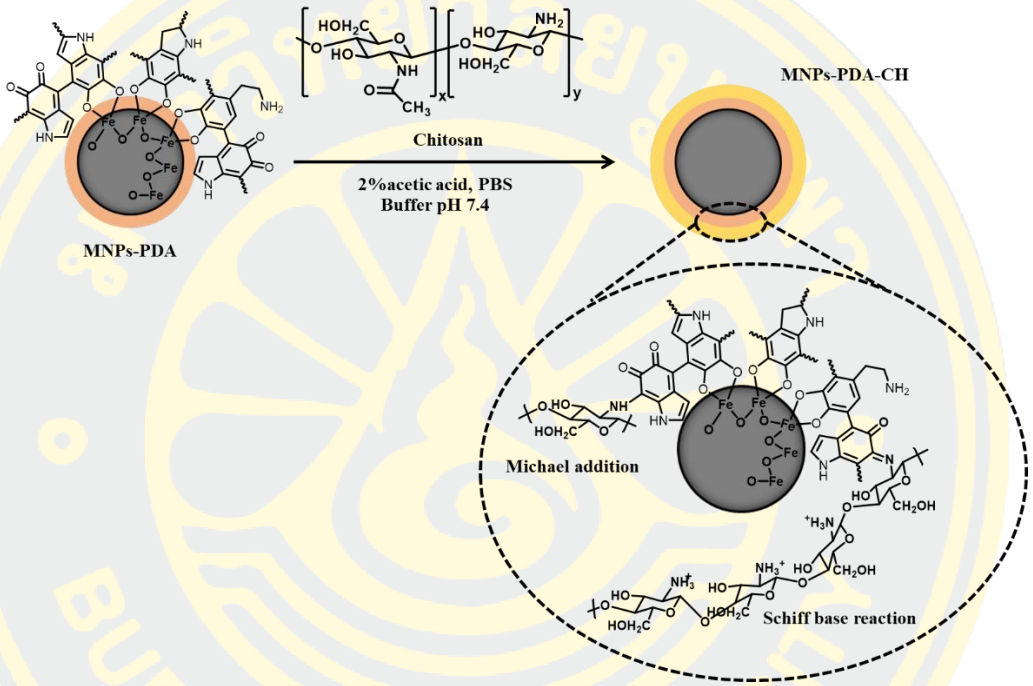

Figure 4-17 Illustrates the preparation of chitosan-modified MNPs-PDA (MNPs-PDA-CH)

Figure 4-18 displays the ATR-FTIR spectrum of MNPs-PDA-CH with various concentrations of chitosan. A new peak at 1066 cm^{-1}, corresponding to the C-O-C stretching vibration of the polysaccharide backbone in chitosan, was observed. This observation leads to the conclusion that chitosan is indeed anchored on the surface of MNPs-PDA

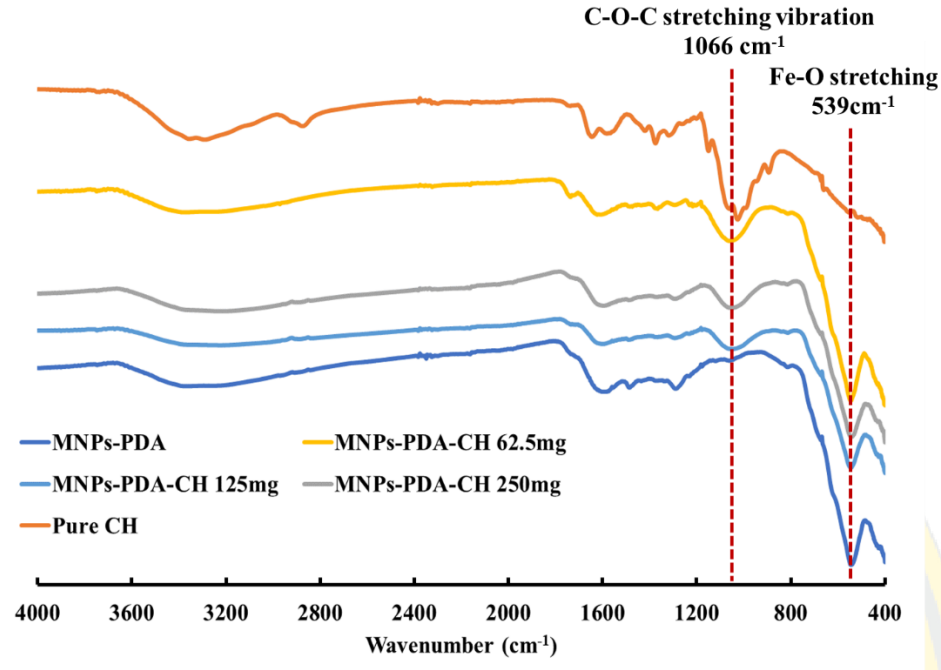

Figure 4-18 ATR-FTIR spectra of MNPs-PDA-CH

The alteration in the surface charge of MNPs-PDA due to chitosan coating was analyzed by measuring the zeta potential of each type of MNP-PDA-CH (Figure 4-19). The surface charges of MNPs-PDA changed from -7.6 mV to +12.1 mV, indicating that the negative charge of MNPs-PDA was reduced by the presence of chitosan. These results suggest that positively charged molecules such as chitosan can reduce the negative charge on the surface of MNPs-PDA.

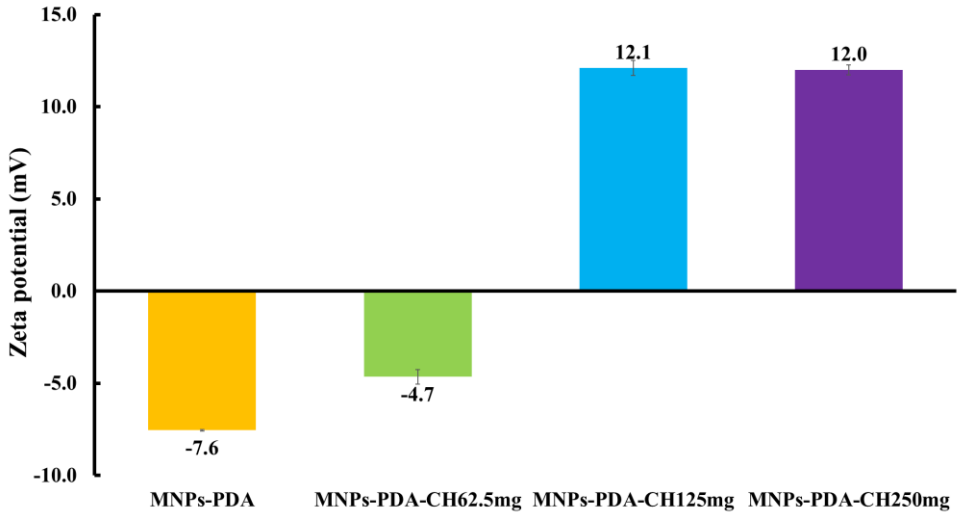

Figure 4-19 Zeta potential analysis of optimum concentration with chitosan

Figure 4-20 shows the TEM images of MNPs-PDA-CH with various concentrations of chitosan. It was observed that MNPs-PDA-CH formed clusters of nanoparticles. However, the size of the clusters appeared to decrease with increasing chitosan concentration. This finding is consistent with the DLS measurements (Figure 4-21).

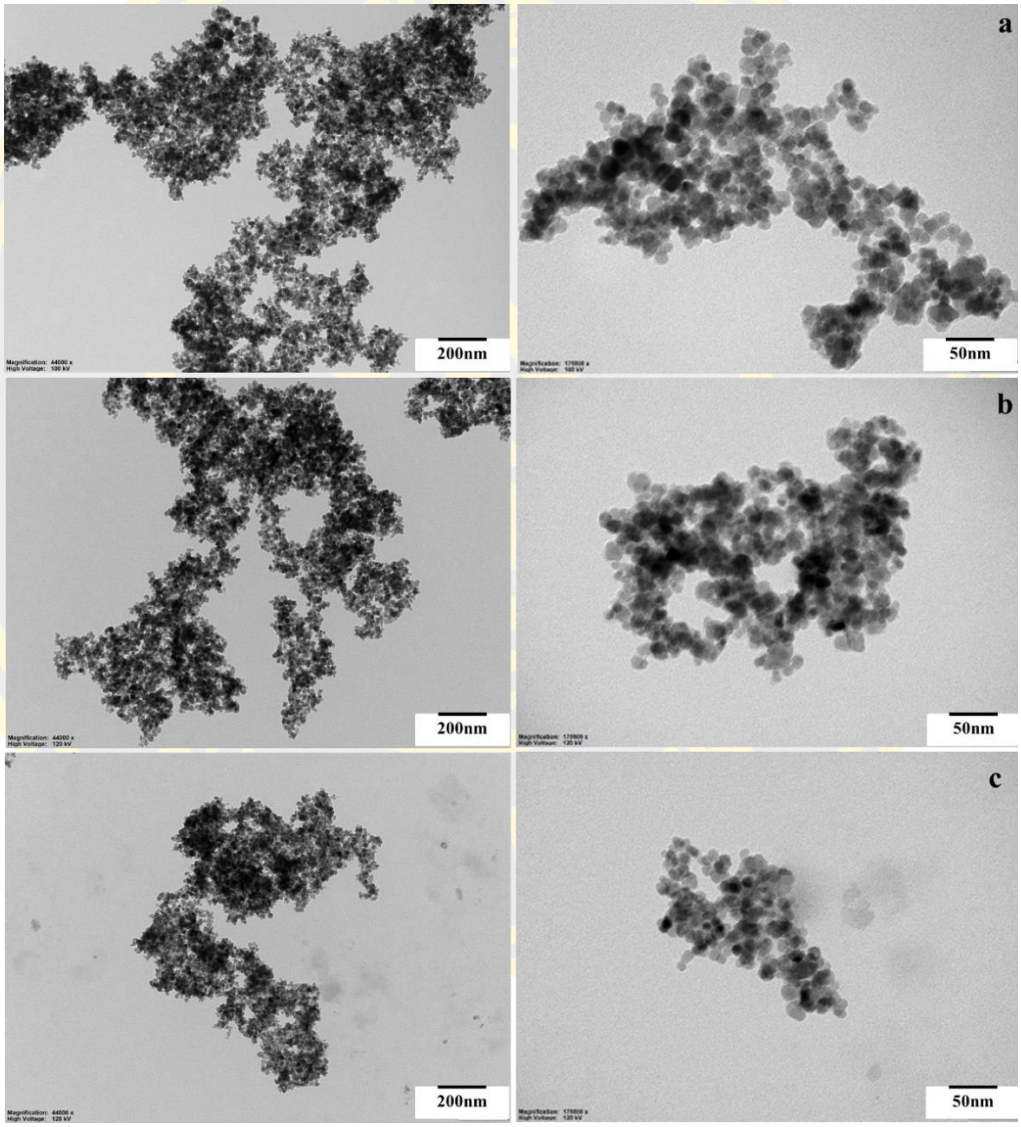

Figure 4-20 TEM image of (a) MNPs-PDA-CH 62.5 mg, (b) MNPs-PDA-CH 125 mg and (c) MNPs-PDA-CH 250 mg

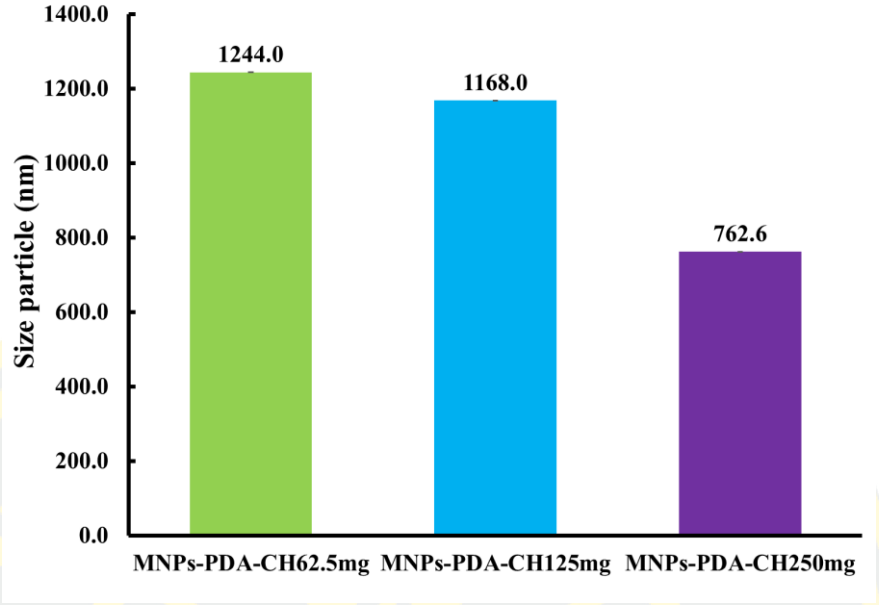

Figure 4-21 Hydrodynamic diameter of optimum concentration.

4.4. Isoelectric Point Determination of MNPs-CH and MNPs-PDA-CH

The zeta potential of MNPs-CH and MNPs-PDA-CH was measured across various pH solutions, ranging from 3 to 9 (Figure 4-22). Both MNPs-CH and MNPs-PDA-CH exhibited an isoelectric point (IEP) around pH ≈ 5.5. Below this pH, the amino groups on their surfaces were protonated, resulting in a positive charge. Conversely, as the pH exceeded the IEP, the charge became negative. The introduction of chitosan led to MNPs-CH and MNPs-PDA-CH carrying positive charges at pH levels below 5.5. These findings illustrate chitosan's effective role in modifying MNPs to confer positive charge properties. Thus, the MNPs-CH and MNPs-PDA-CH are suitable for use as materials for bacteria capture, as the negatively charged bacterial membrane can interact with the positively charged chitosan on the surface of MNPs-CH and MNPs-PDA-CH.

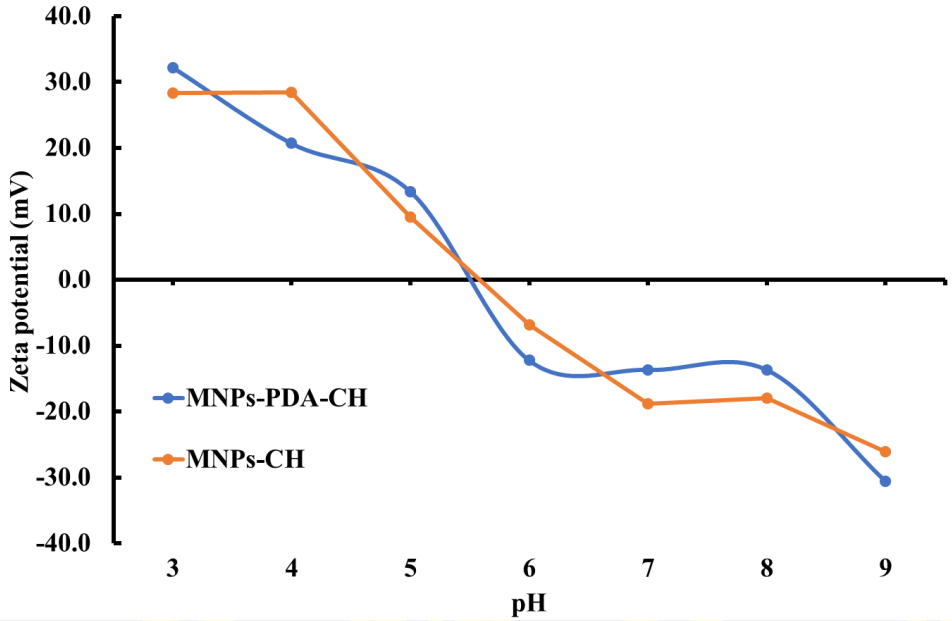

Figure 4-22 Isoelectric point of MNPs-CH and MNPs-PDA-CH

4.5 The study of bacteria separation

In the following work, the separation of bacteria with MNPs-CH and MNPs-PDA-CH was evaluated. *E. coli* (Gram-negative bacteria) and *S. aures* (Gram-positive bacteria bacteria) were selected in this experiment.

Figure 4-23 shows the effect of pH on the separation efficiency. It was observed that at pH 5.0, a high separation efficiency was achieved for both types of bacteria, while at pH 7.4, a very low separation efficiency was observed. This effect may be attributed to the acidic pH causing chitosan to exhibit a more positive charge compared to at pH 7.4. Thus, it induces the electrostatic interaction between the positively charged chitosan on the surface of MNPs-CH and MNPs-PDA-CH and the negatively charged surface, as well as outer-core lipopolysaccharides, of the bacterial membrane.

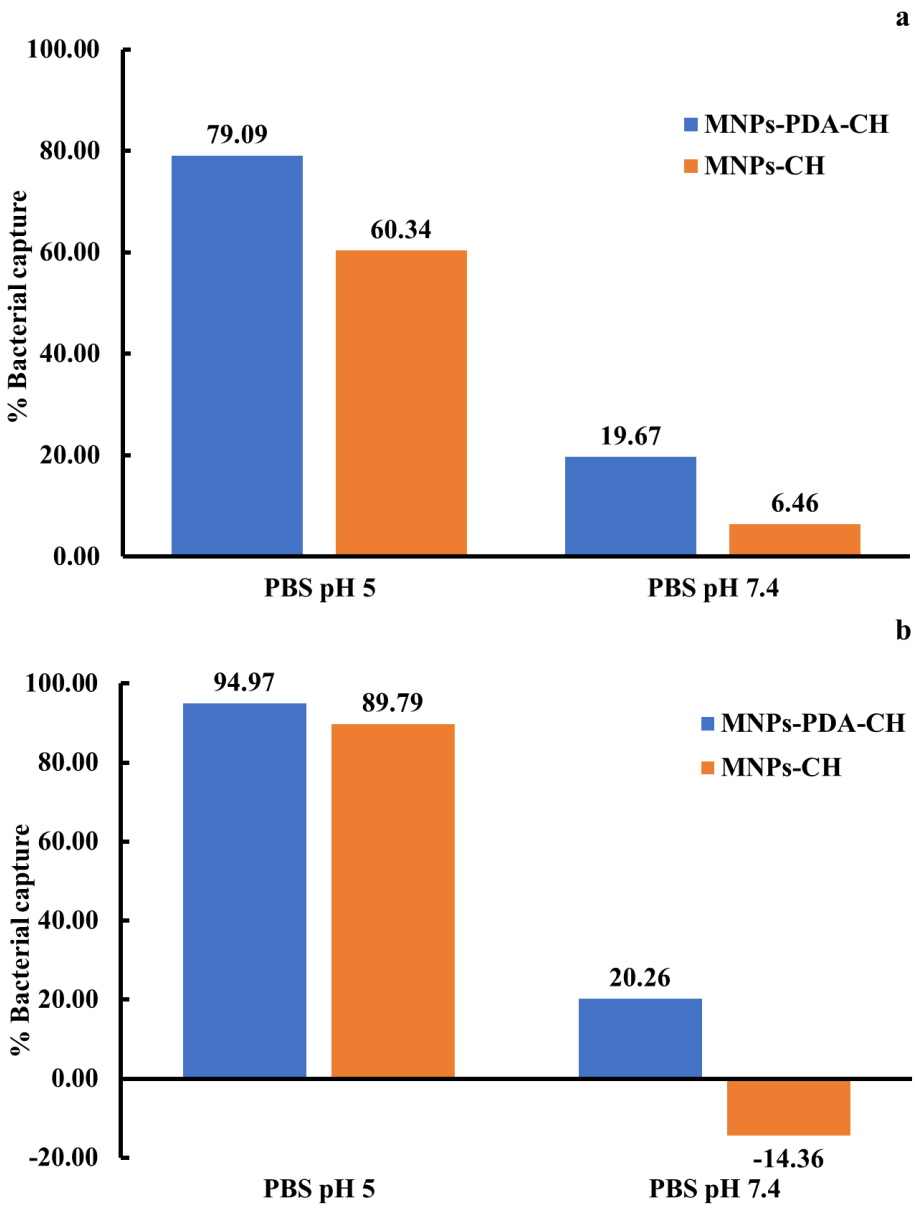

Figure 4-23 Effect of pH buffer of PBS (a) *E.coli* and (b) *S. aureus*

Figure 4-24 shows the effect of chitosan concentration on the separation efficiency. In the case of MNPs-CH, the separation efficiency trended to increase with increasing chitosan concentration for both types of bacteria and saturated at 125 mg of chitosan. Thus MNPs-CH with 125 mg of chitosan are the best for use as materials for bacteria capture in future studies. Additionally, in the case of MNPs-PDA-CH, it was observed that at 125 mg, it also showed high separation efficiency for both types of bacteria.

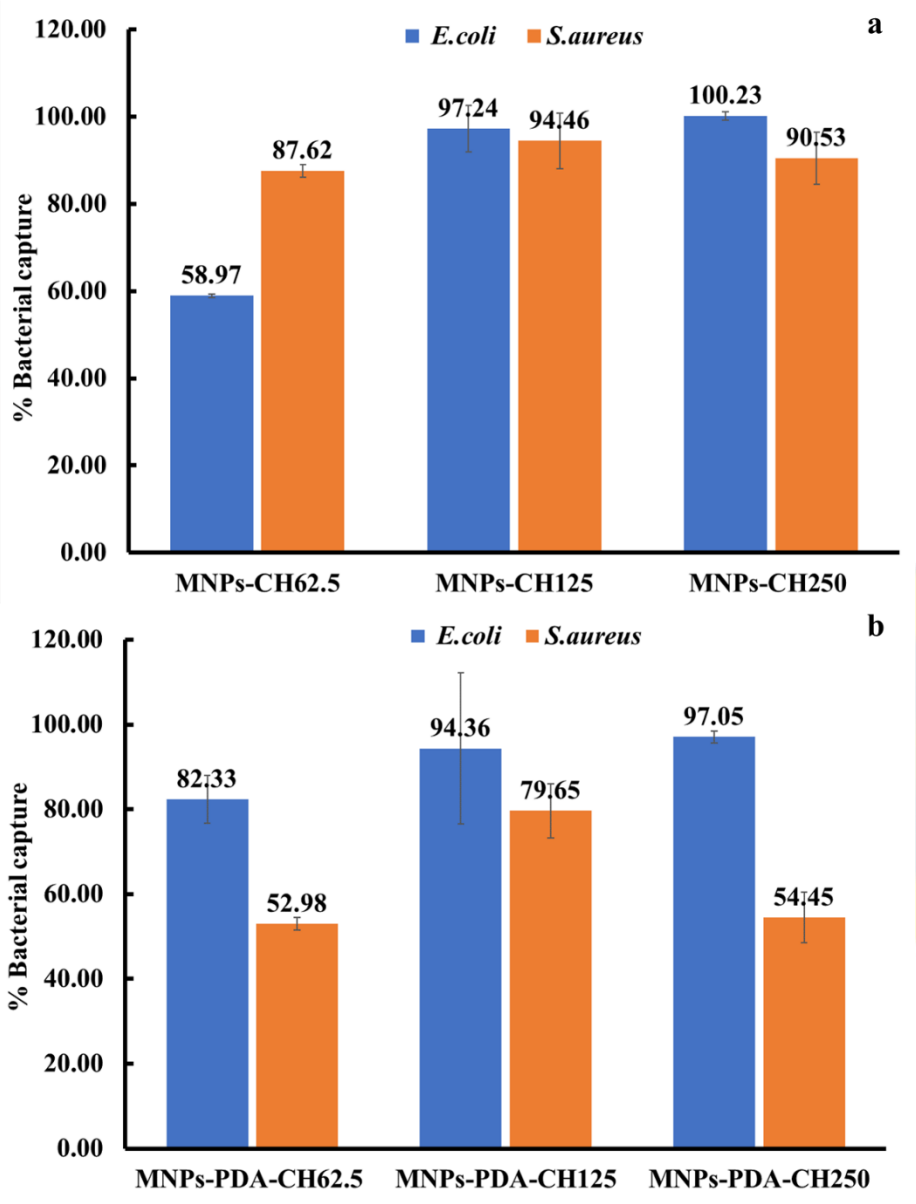

Figure 4-24 Effect of chitosan concentration on the separation efficiency (a) MNPs-CH and (b) MNPs-PDA-CH.

4.6 The study of bacteria detection

In this section, the concept of detection is based on an integrated approach, involving the capture of bacteria with MNPs and the monitoring of glucose consumption by captured bacteria using a portable glucose meter (PGMs) as a signal readout. The change in glucose concentration serves as the detection signal (Figure 4-25). If bacteria are present in the sample, they will consume glucose, resulting in a detectable change in glucose concentration.

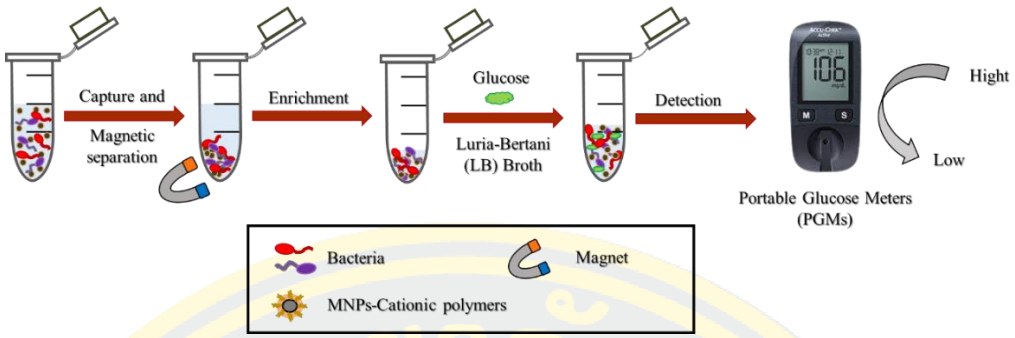

Figure 4-25 The capture of bacteria with MNPs and the monitoring of glucose consumption by captured bacteria using a portable glucose meter (PGMs) as a signal readout.

On this basis, the change in glucose levels of the MNPs conjugate to *E. coli* and *S. aureus* was investigated. Figures 4-26a and 4-26b illustrate the change in glucose concentrations over time, demonstrating the reduction in glucose levels by *E. coli* and *S. aureus* (green line). In contrast, in the absence of bacteria (control), there is no drop in glucose concentrations over six hours (blue line). This indicates that the captured bacteria demonstrated the ability for glucose consumption, resulting in a decrease in glucose concentration and providing evidence of the success of this detection concept.

To investigate the efficacy of magnetic separation step, the detection without the step of bacteria capture with MNPs was evaluated. In the case without the step of bacteria capture, a decrease in glucose concentrations over time was also observed (orange line) due to the glucose consumption by bacteria. However, the time required to observe a significant drop in glucose concentrations is longer compared to the case with the step of bacteria capture. These results indicate that capturing bacteria with MNPs provides enrichment of bacteria, resulting in improved detection efficiency in a short period of time.

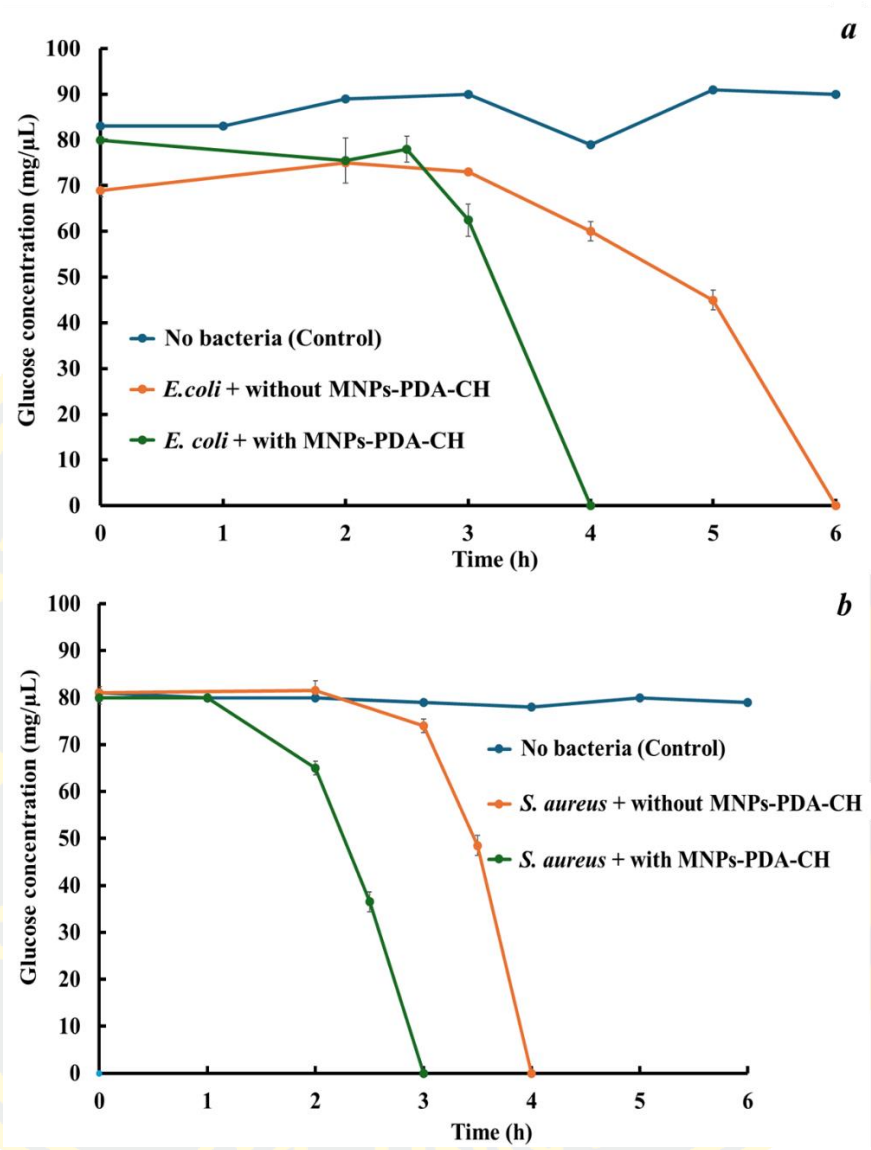

Figure 4-26 The change in glucose levels in the reaction solution monitored over time by PMG. (a) *E. coli* and (b) *S. aureus*.

4.6.1 Optimization of experiment parameters

4.6.1.1 Effect of nanoparticles type

Three types of nanoparticles, namely MNPs-CH, MNPs-PDA, and MNPs-PDA-CH were used to study the efficacy of *E. coli* and *S. aureus* detection. Figures 4-27a and 4-27b show a drop in PMG readings indicative of glucose consumption by *E. coli* and *S. aureus,* respectively, recorded over time, demonstrating a gradual decrease in glucose levels with all types of nanoparticles. However, when considering the rate of glucose consumption (%ΔC), it was found that MNPs-PDA-CH exhibited the

highest %ΔC for both *E. coli* and *S. aureus* (Figures 4-28a and 4-28b), corresponding to provide the highest responding signal. Therefore, the MNPs-PDA-CH appears to be useful for bacterial detection.

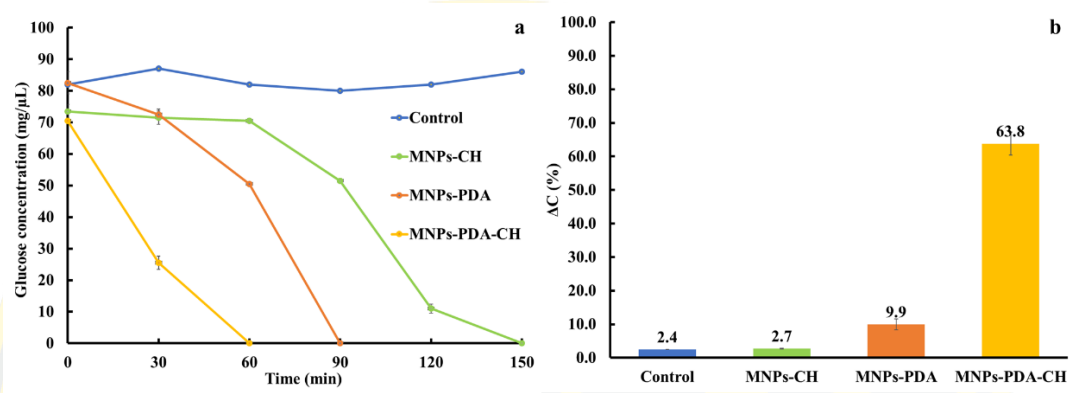

Figure 4-27 (a) Drop in PMG readings consumption by *E. coli* recorded over time for different types of nanoparticles. (b) Comparison of the %ΔC for different types of particles at 30-minute of detection time.

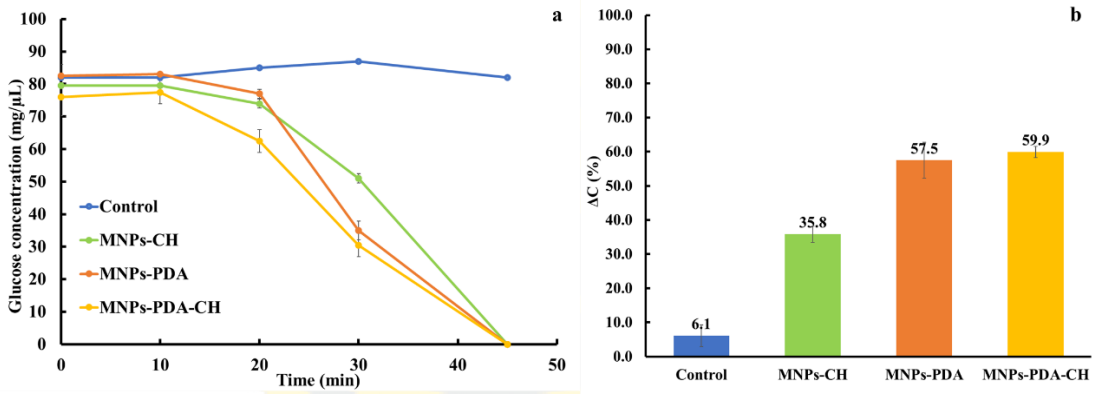

Figure 4-28 (a) Drop in PMG readings consumption by *S. aureus* recorded over time for different types of particles. (b) Comparison of the %ΔC for different types of particles at 30-minute of detection time.

4.6.1.2 Effect of nanoparticles amount

Figures 4-29 and 4-30 demonstrated the effect of nanoparticles amount. The results show that in case of *E coli*, the %ΔC trended increase with the dosage of nanoparticles. However, for *S. aureus,* %ΔC did not exhibit a significant increase with increasing the amount of nanoparticles. To achieve the best detection for both *E. coli* and *S. aureus,* nanoparticles amount of 1.0 mg is chosen.

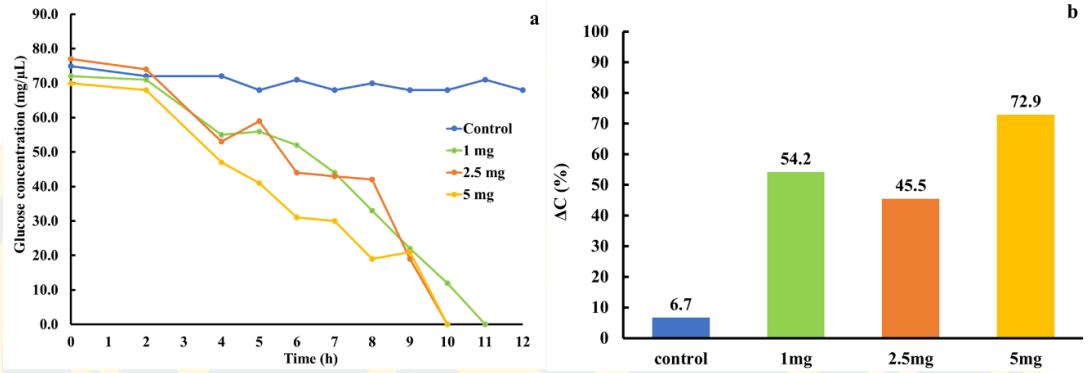

Figure 4-29 (a) Drop in PMG readings consumption by *E. coli* recorded over time for different MNPs dosages. (b) Comparison of the %ΔC for different MNPs dosages at 8 hours of detection time.

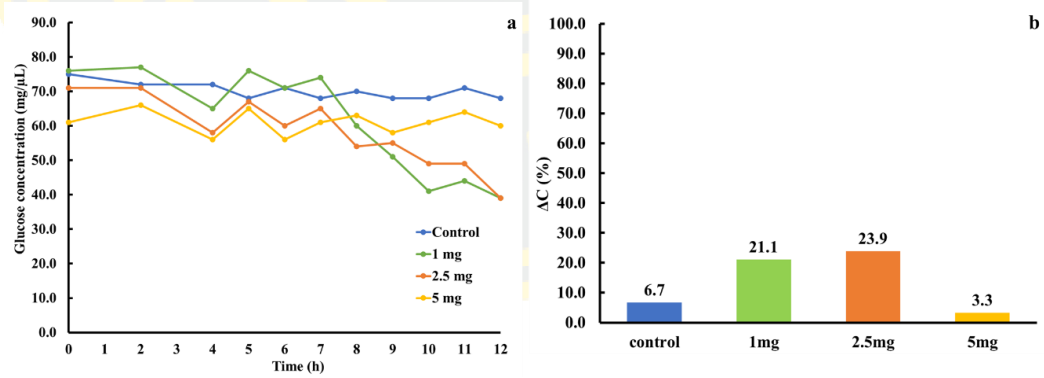

Figure 4-30 (a) Drop in PMG readings consumption by *S. aureus* recorded over time different MNPs dosages. (b) Comparison of the %ΔC for different MNPs dosages at 8 hours of detection time.

4.6.1.3 Effect of the sample volume

As shown in Figures 4-31 and 4-32, a low sample volume exhibits a slow change in glucose concentration. The %ΔC gradually increases with the increase in sample volume from 1.0 mL to 10.0 mL. This is because a larger sample volume leads to an increased number of bacteria in the sample solution, resulting in a higher signal of change.

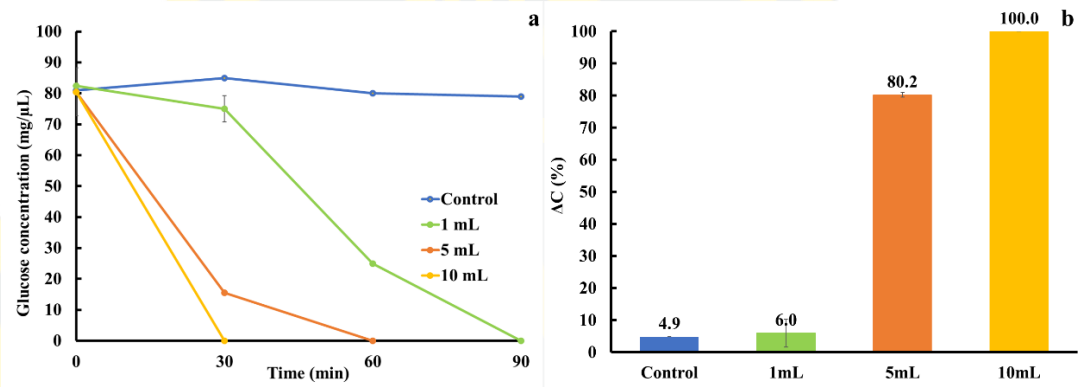

Figure 4-31 (a) Drop in PMG readings consumption by *E. coli* recorded over time for different sample volume. (b) Comparison of the %ΔC for different sample volume at 30-minute of detection time.

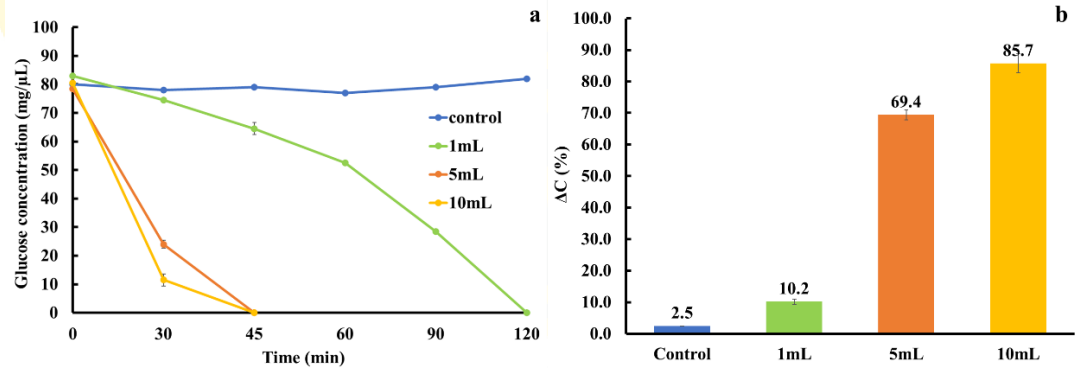

Figure 4-32 (a) Drop in PMG readings consumption by *S. aureus* recorded over time for different sample volume. (b) Comparison of the %ΔC for different sample volume at 30-minute of detection time.

4.6.1.4 Effect of incubation time of MNPs-PDA-CH with bacteria

In this experiment, the effect of incubation time of MNPs-PDA-CH with bacteria was studied at 15, 30, and 45 minutes (Figure 4-33 and 4-34). The results of the experiment show that the incubation time affects the detection efficiency. Longer contact times tended to provide a higher signal of change. However, in the case of *S. aureus*, as its incubation time continued to increase, %ΔC did not show a significant increase. Therefore, incubating MNPs-PDA-CH with *E. coli* and *S. aureus* for 30 minutes appears to be the best condition.

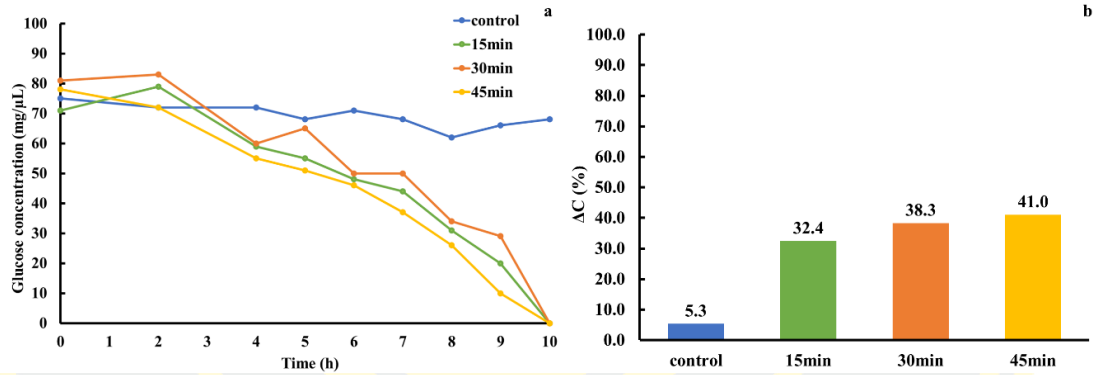

Figure 4-33 (a) Declining in PMG readings consumption by *E. coli* recorded over time for different incubation time of MNPs-PDA-CH with bacteria. (b) Comparison of the %ΔC for different incubation time of MNPs-PDA-CH with bacteria at 6 hours of detection time.

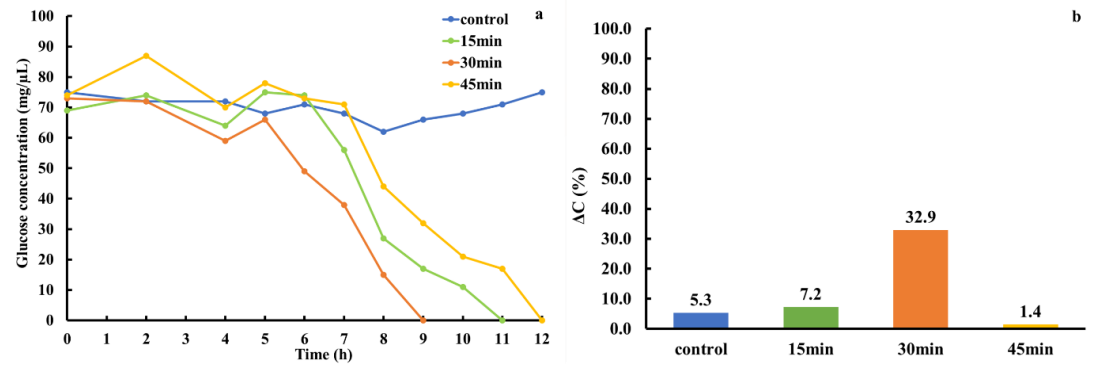

Figure 4-34 (a) Declining in PMG readings consumption by *S. aureus* recorded over time for different incubation time of MNPs-PDA-CH with bacteria. (b) Comparison of the %ΔC for different incubation time of MNPs-PDA-CH with bacteria at 6 hours of detection time.

4.7 The study of bacteria detection in real sample

The real application value of this developed detection method can be revealed by its effectiveness in real samples. We verified the detection performance of this method for food samples using the conventional standard addition method. The dried shrimp sample was spiked with *E. coli* and *S. aureus* at different concentrations (10^1–10^8 CFU/mL) of bacteria to prepare an artificially contaminated dried shrimp sample. The samples were then analyzed using the developed method as follows: they were soaked in PBS buffer (10 mM, pH 5.0), after which 5.0 mL of the sample solution was withdrawn and incubated with 1.0 mg of MNPs-PDA-CH for 30 minutes to form a complex of MNPs-PDA-CH-bacteria. Subsequently, this complex was redispersed in 100 µL of Luria-Bertani broth (LB) containing 10 µL of 1% w/v glucose. The reaction mixture was then incubated at 37 °C. Bacterial detection was completed by measuring the glucose concentration over time using a PMG.

4.7.1 Detection of E. coli in dried shrimp

Figure 4-35 displays the detection results of *E. coli* in dried shrimp samples. The change in glucose concentrations over time was observed; however, the time required to observe a significant drop in glucose concentrations consistently changed with the increase in *E. coli* concentration. As the concentrations of *E. coli* increased, the time required gradually decreased, showing a good linear relationship ($R^2 = 0.9847$) between the time required and the corresponding *E. coli* concentrations in the range of 10^2–10^7 CFU/mL (Figure 4-36). The lowest concentration of *E. coli* in dried shrimp was 3.25×10^1 CFU/mL

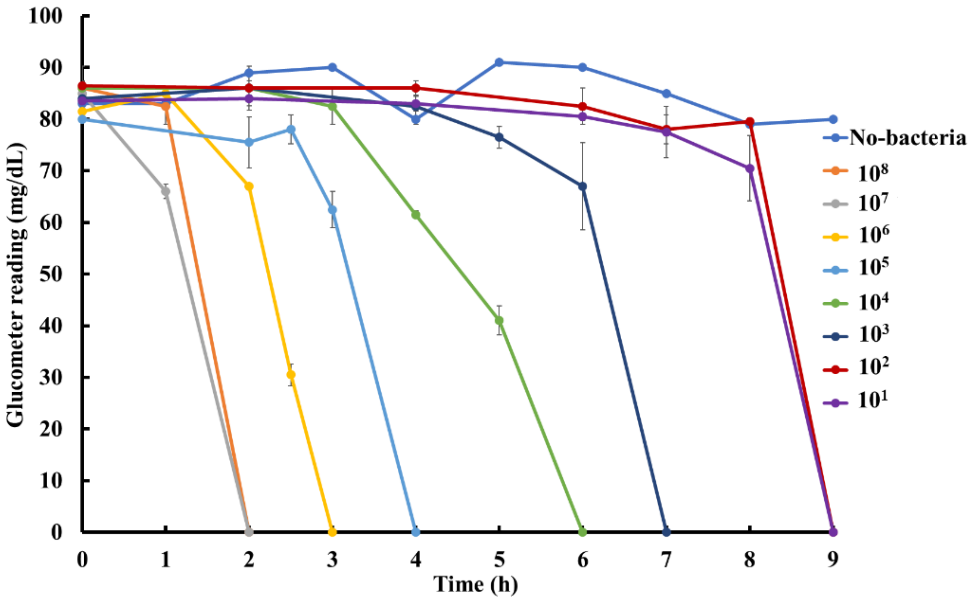

Figure 4-35 The change in glucose levels in the reaction solution monitored over time by PMG. The concentration of *E. coli* ranging from 3.25×10^1 - 3.25×10^8 CFU/mL.

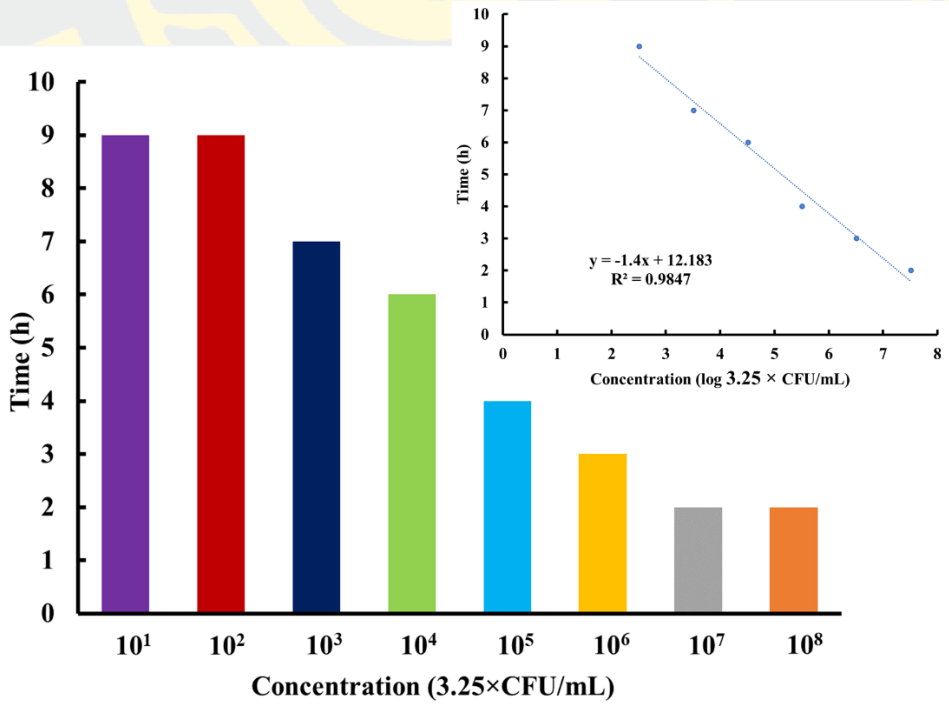

Figure 4-36 Time needed to detect a significant decrease in glucose concentrations at various concentrations of *E. coli* ranging from 3.25×10^1 – 3.25×10^8 CFU/mL.

4.7.1 Detection of S. aureus in dried shrimp

Figure 4-37 displays the detection results of *S. aureus* in dried shrimp samples. The change in glucose concentrations over time was observed; however, the time required to observe a significant drop in glucose concentrations consistently changed with the increase in *S. aureus* concentration. As the concentrations of *S. aureus* increased, the time required gradually decreased, showing a good linear relationship ($R^2 = 0.9878$) between the time required and the corresponding *S. aureus* concentrations, establishing standard curves (Figure 4-38). These results showed good detection performance for 10^1–10^8 CFU/mL of *S. aureus* in dried shrimp. The lowest concentration of *S. aureus* in dried shrimp was 2.85 x 10^1 CFU/mL

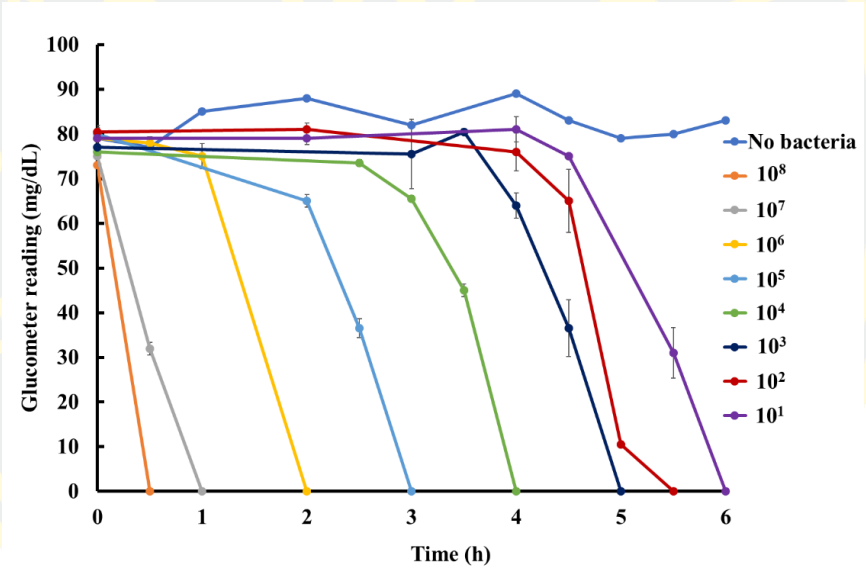

Figure 4-37 The change in glucose levels in the reaction solution monitored over time by PMG. The concentration of *S. aureus* ranging from 2.85 × 10^1 - 2.85 × 10^8 CFU/mL.

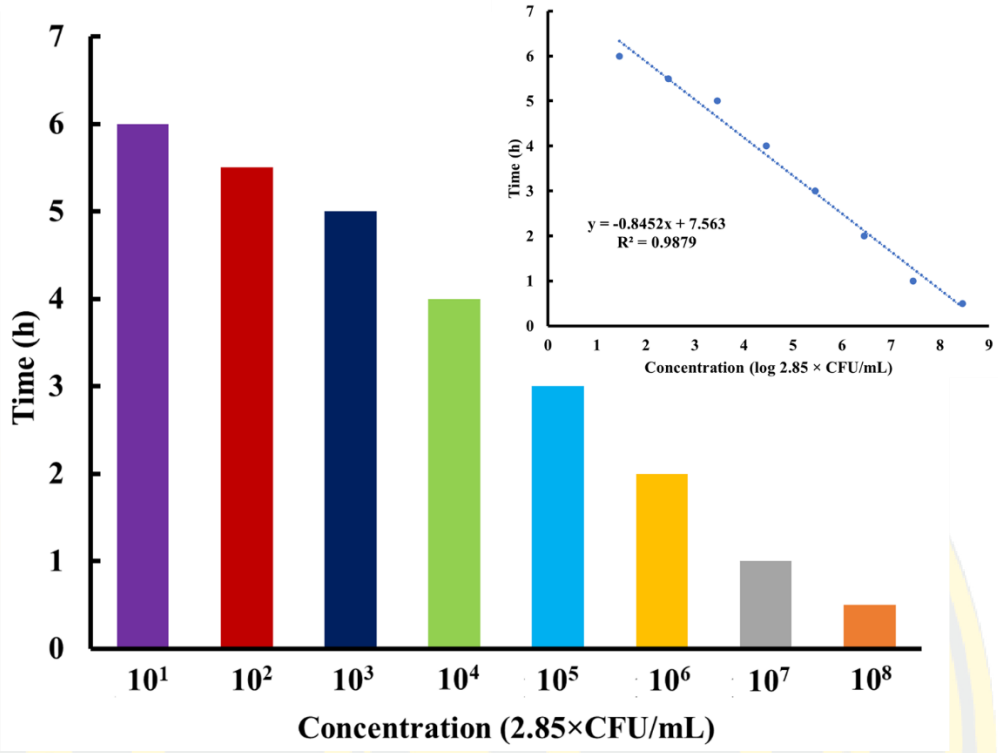

Figure 4-38 Time needed to detect a significant decrease in glucose concentrations at various concentrations of *S. aureus* ranging from 2.85×10^1 - 2.85×10^8 CFU/mL.

4.8 Method validation

To evaluate accuracy, this method was compared with the classical plate culture method for detecting 20 samples of dried shrimp and dried squid purchased from Nong Mon Market. As shown in Table 4.1, a total of 20 samples (including 14 positive and 6 negative samples) were identified by the plate culture method, and then tested using our developed method. The results revealed one false negative result among the analysis of 14 positive samples and zero false positive results among the analysis of 6 negative samples (physical images of the actual results are shown in Tables 4.2 and 4.3). It was calculated that the sensitivity, specificity, and accuracy of this method were 93%, 100%, and 95%, respectively

Table 4-1 Performance evaluation of total bacteria count in real samples.

Our method	Plate culture			Sensitivity	Specificity	Accuracy
	Positive (n=14)	Negative (n=6)	Total (n=20)			
Positive	13	0	13	13/14 (93%)	/	19/20 (95%)
Negative	1	6	7	/	6/6 (100%)	

Table 4-2 Results of testing efficiency for measuring total bacteria in dried ink samples. Comparison between the standard method (plate culture) and the new method for measuring bacteria (our method)

Method validation	**Plate culture**		**Our method ΔC (%)/hours**	
Dried squid	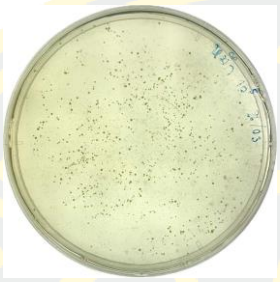	Positive result (+)	Positive result (+)	100%/ 6h
	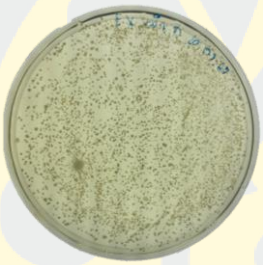	Positive result (+)	Positive result (+)	21.7%/ 7h
		Positive result (+)	Positive result (+)	14.9%/ 7h
	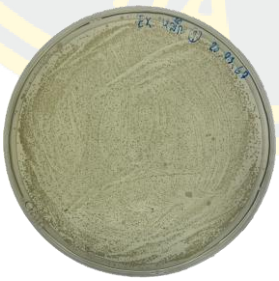	Positive result (+)	Positive result (+)	7.4%/ 7h
		Negative result (-)	Negative result (-)	0%/ 9h

Method validation	Plate culture		Our method ΔC (%)/hours	
Dried squid	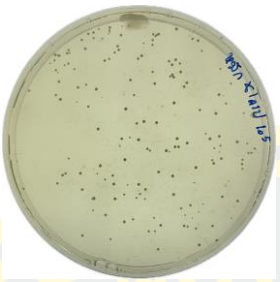	Positive result (+)	Negative result (-)	0%/ 9h
	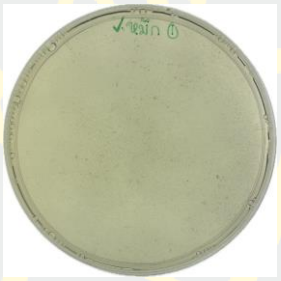	Negative result (-)	Negative result (-)	0%/ 9h
	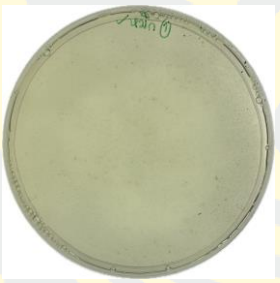	Negative result (-)	Negative result (-)	0%/ 9h
	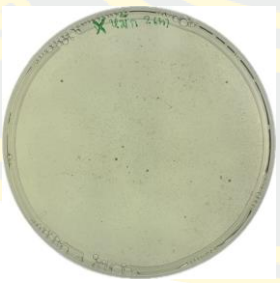	Positive result (+)	Positive result (+)	14%/ 9h
		Positive result (+)	Positive result (+)	100%/8h

Table 4-3 Results of testing efficiency for measuring total bacteria in dried shrimp samples. Comparison between the standard method (plate culture) and the new method for measuring bacteria (our method)

Method validation	**Plate culture**		**Our method ΔC (%)/hours**	
Dried shrimp		Positive result (+)	Positive result (+)	100%/ 6h
		Positive result (+)	Positive result (+)	100%/ 5h
		Positive result (+)	Positive result (+)	100%/ 7h
		Positive result (+)	Positive result (+)	100%/ 7h
	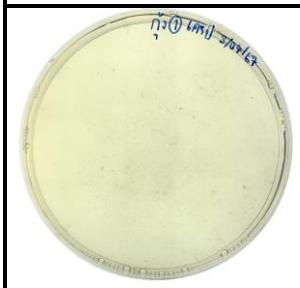	Negative result (-)	Negative result (-)	0%/ 9h

Method validation	Plate culture		Our method ΔC (%)/hours	
Dried shrimp	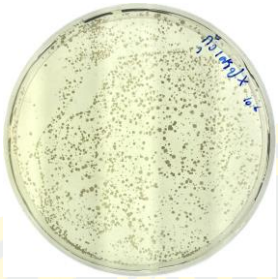	Positive result (+)	Positive result (+)	100%/ 7h
	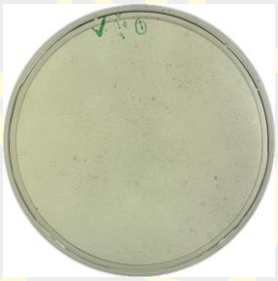	Negative result (-)	Negative result (-)	0%/ 9h
	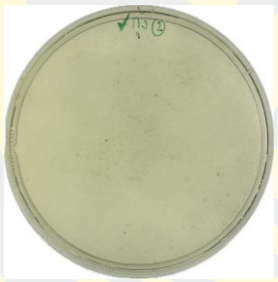	Negative result (-)	Negative result (-)	0%/ 9h
	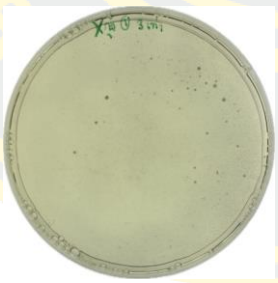	Positive result (+)	Positive result (+)	100%/ 6h
		Positive result (+)	Positive result (+)	100%/ 6h

CHAPTER 5
CONCLUSION AND DISCUSSION

In summary, MNPs were successfully synthesized and modified with the positively charged polymer chitosan using two approaches: 1) electrostatic adsorption (MNPs-CH) and 2) chemical bonding (MNPs-PDA-CH). Both the positively charged MNPs-CH and MNPs-PDA-CH exhibited outstanding capture ability for both gram-negative *Escherichia coli* and gram-positive *Staphylococcus aureus* (> 50%) through electrostatic interaction. The captured bacteria displayed glucose consumption, with the decrease in glucose concentration detectable using a portable glucose meter (PGM). The detection of both gram-negative and gram-positive in dried shrimp samples revealed a good linear correlation between the time needed to detect a significant decrease in glucose concentrations and bacteria concentration. The established detection procedure demonstrates a simple and low-cost method based on remarkable bacteria separation and glucose consumption.

REFERENCES

Agyarkwa, M. A., Azaglo, G. S. K., Kokofu, H. K., Appah-Sampong, E. K., Nerquaye-Tetteh, E. N., Appoh, E., . . . Opintan, J. A. (2022). Surveillance of WHO Priority Gram-Negative Pathogenic Bacteria in Effluents from Two Seafood Processing Facilities in Tema, Ghana, 2021 and 2022: A Descriptive Study. *Int J Environ Res Public Health, 19*(17). doi:10.3390/ijerph191710823

Ali, A., Zafar, H., Zia, M., Ul Haq, I., Phull, A. R., Ali, J. S., & Hussain, A. (2016). Synthesis, characterization, applications, and challenges of iron oxide nanoparticles. *Nanotechnol Sci Appl, 9*, 49-67. doi:10.2147/NSA.S99986

Augustine, R., Abraham, A. R., Kalarikkal, N., & Thomas, S. (2016). Monitoring and separation of food-borne pathogens using magnetic nanoparticles. In *Novel Approaches of Nanotechnology in Food* (pp. 271-312).

Chavali, R., Kumar Gunda, N. S., Naicker, S., & Mitra, S. K. (2014). Detection of Escherichia coli in potable water using personal glucose meters. *Analytical Methods, 6*(16). doi:10.1039/c4ay01249f

Che, Y., Xu, Y., Wang, R., & Chen, L. (2017). Rapid fluorescence detection of pathogenic bacteria using magnetic enrichment technique combined with magnetophoretic chromatography. *Anal Bioanal Chem, 409*(20), 4709-4718. doi:10.1007/s00216-017-0415-6

Clausen, C. H., Dimaki, M., Bertelsen, C. V., Skands, G. E., Rodriguez-Trujillo, R., Thomsen, J. D., & Svendsen, W. E. (2018). Bacteria Detection and Differentiation Using Impedance Flow Cytometry. *Sensors (Basel), 18*(10). doi:10.3390/s18103496

Davodi, B., Jahangiri, M., & Ghorbani, M. (2018). Magnetic Fe3O4@ polydopamine biopolymer: Synthesis, characterization and fabrication of promising nanocomposite. *Journal of Vinyl and Additive Technology, 25*(1), 41-47. doi:10.1002/vnl.21627

Fang, W., Han, C., Zhang, H., Wei, W., Liu, R., & Shen, Y. (2016). Preparation of amino-functionalized magnetic nanoparticles for enhancement of bacterial capture efficiency. *RSC Advances, 6*(72), 67875-67882. doi:10.1039/c6ra13070d

Joo, J., Kwon, D., Shin, H. H., Park, K.-H., Cha, H. J., & Jeon, S. (2013). A facile and sensitive method for detecting pathogenic bacteria using personal glucose meters. *Sensors and Actuators B: Chemical, 188*, 1250-1254. doi:10.1016/j.snb.2013.08.027

Kuchma, E., Kubrin, S., & Soldatov, A. (2018). The Local Atomic Structure of Colloidal Superparamagnetic Iron Oxide Nanoparticles for Theranostics in Oncology. *Biomedicines, 6*(3). doi:10.3390/biomedicines6030078

Kumar, H., Bhardwaj, K., Kaur, T., Nepovimova, E., Kuca, K., Kumar, V., . . . Kumar, D. (2020). Detection of Bacterial Pathogens and Antibiotic Residues in Chicken Meat: A Review. *Foods, 9*(10). doi:10.3390/foods9101504

Kwon, D., Lee, H., Yoo, H., Hwang, J., Lee, D., & Jeon, S. (2018). Facile method for enrofloxacin detection in milk using a personal glucose meter. *Sensors and Actuators B: Chemical, 254*, 935-939. doi:10.1016/j.snb.2017.07.118

Lamaoui, A., Palacios-Santander, J. M., Amine, A., & Cubillana-Aguilera, L. . (2021). Molecularly imprinted polymers based on polydopamine: Assessment of non-specific adsorption. *Microchemical Journal, 164*.

doi:10.1016/j.microc.2021.106043
Li, Q., Xie, G., Wang, Y., Aguilar, Z. P., & Xu, H. (2021). Vancomycin-modified poly-l-lysine magnetic separation combined with multiplex polymerase chain reaction assay for efficient detection of Bacillus cereus in milk. *J Dairy Sci, 104*(2), 1465-1473. doi:10.3168/jds.2020-18962
Li, Z., Ma, J., Ruan, J., & Zhuang, X. (2019). Using Positively Charged Magnetic Nanoparticles to Capture Bacteria at Ultralow Concentration. *Nanoscale Res Lett, 14*(1), 195. doi:10.1186/s11671-019-3005-z
Meng, X., Li, F., Li, F., Xiong, Y., & Xu, H. (2017). Vancomycin modified PEGylated-magnetic nanoparticles combined with PCR for efficient enrichment and detection of Listeria monocytogenes. *Sensors and Actuators B: Chemical, 247*, 546-555. doi:10.1016/j.snb.2017.03.079
Moffa, M. A., Bremmer, D. N., Carr, D., Buchanan, C., Shively, N. R., Elrufay, R., & Walsh, T. L. (2020). Impact of a Multiplex Polymerase Chain Reaction Assay on the Clinical Management of Adults Undergoing a Lumbar Puncture for Suspected Community-Onset Central Nervous System Infections. *Antibiotics (Basel), 9*(6). doi:10.3390/antibiotics9060282
Mrówczyński, R., Jurga-Stopa, J., Markiewicz, R., Coy, E. L., Jurga, S., & Woźniak, A. (2016). Assessment of polydopamine coated magnetic nanoparticles in doxorubicin delivery. *RSC Advances, 6*(7), 5936-5943. doi:10.1039/c5ra24222c
Oroujeni, M., Kaboudin, B., Xia, W., Jönsson, P., & Ossipov, D. A. (2018). Conjugation of cyclodextrin to magnetic Fe3O4 nanoparticles via polydopamine coating for drug delivery. *Progress in Organic Coatings, 114*, 154-161. doi:10.1016/j.porgcoat.2017.10.007
Salazar, P., Martín, M., & González-Mora, J. (2016). <Polydopamine-modified surfaces in biosensor applications.pdf>.
Xiao, F., Bai, X., Wang, K., Sun, Y., & Xu, H. (2022). Rapid-Response Magnetic Enrichment Strategy for Significantly Improving Sensitivity of Multiplex PCR Analysis of Pathogenic Listeria Species. *Applied Sciences, 12*(13). doi:10.3390/app12136415
Xu, C., Chen, F., Valdovinos, H. F., Jiang, D., Goel, S., Yu, B., . . . Cai, W. (2018). Bacteria-like mesoporous silica-coated gold nanorods for positron emission tomography and photoacoustic imaging-guided chemo-photothermal combined therapy. *Biomaterials, 165*, 56-65. doi:10.1016/j.biomaterials.2018.02.043
Ye, L., Zhao, G., & Dou, W. (2017). An ultrasensitive sandwich immunoassay with a glucometer readout for portable and quantitative detection of Cronobacter sakazakii. *Analytical Methods, 9*(44), 6286-6292. doi:10.1039/c7ay02222k
Zhang, Y., Du, B., Wu, Y., Liu, Z., Wang, J., Xu, J., . . . Liu, B. (2022). Fe(3)O(4)@PDA@PEI Core-Shell Microspheres as a Novel Magnetic Sorbent for the Rapid and Broad-Spectrum Separation of Bacteria in Liquid Phase. *Materials (Basel), 15*(6). doi:10.3390/ma15062039

มหาวิทยาลัยบูรพา
BURAPHA UNIVERSITY

BIOGRAPHY

NAME	Kamonluck Witthayasutthaphon
DATE OF BIRTH	14 August 2000
PLACE OF BIRTH	Rayong
PRESENT ADDRESS	7/124 Lumpini, Pathumwan, Rama 4 Road, Bangkok 10330
EDUCATION	2018-2021 Bachelor Science of Chemistry (B.Sc), Faculty of Science, Burapha University, Thailand